Quaternary Science Reviews 292 (2022) 107638

Contents lists available at ScienceDirect

Quaternary Science Reviews

journal homepage: www.elsevier.com/locate/quascirev

Hunter-gatherer environments at the Late Pleistocene sites of Mwanganda's Village and Bruce, northern Malawi

Flora Schilt [a, b, *], Christopher E. Miller [a, c], David K. Wright [d, e], Susan M. Mentzer [a, f], Julio Mercader [g, h, i], Patrick Moss [j], Jeong-Heon Choi [k], Gunnar Siljedal [g], Siobhán Clarke [g], Aloyce Mwambwiga [g, l], Kelly Thomas [g], Alvise Barbieri [b], Potiphar Kaliba [m], Elizabeth Gomani-Chindebvu [n], Jessica C. Thompson [o, p]

[a] Institute for Archaeological Sciences and Senckenberg Centre for Human Evolution and Paleoenvironment, University of Tübingen, Tübingen, Germany
[b] Interdisciplinary Center for Archaeology and Evolution of Human Behaviour, University of Algarve, FCHS, Campus Gambelas, Faro, Portugal
[c] SFF Centre for Early Sapiens Behaviour (SapienCE), University of Bergen, Bergen, Norway
[d] Department of Archaeology, Conservation and History, University of Oslo, Oslo, Norway
[e] State Key Laboratory of Loess and Quaternary Geology, Institute of Earth Environment, Chinese Academy of Sciences, Xian, China
[f] School of Anthropology, University of Arizona, Tucson, AZ, USA
[g] Department of Anthropology & Archaeology, University of Calgary, 2500 University Drive NW, Calgary, Alberta, T2N 1N4, Canada
[h] Department of Archaeology, Max Planck Institute for the Science of Human History, Jena, 07745, Germany
[i] Institut Català de Paleoecologia Humana i Evolució Social (IPHES), Zona Educacional, 4 – Campus Sescelades URV (Edifici W3), Tarragona, 43007, Spain
[j] School of Earth and Environmental Sciences, The University of Queensland, Queensland, Brisbane 4072, Australia
[k] Research Center for Geochronology and Isotope Analysis, Korea Basic Science Institute, Ochang, Republic of Korea
[l] National Natural History Museum, PO Box 2160, Arusha, Tanzania
[m] Malawi Department of Museums and Monuments, Lilongwe, Malawi
[n] Ministry of Civic Education and National Unity, Lilongwe, Malawi
[o] Department of Anthropology and Yale Peabody Museum of Natural History, Yale University, New Haven, CT, USA
[p] Institute of Human Origins, P.O. Box 874101, Tempe, AZ 85287, USA

ARTICLE INFO

Article history:
Received 23 March 2022
Received in revised form
28 June 2022
Accepted 30 June 2022
Available online 8 August 2022

Handling Editor: Giovanni Zanchetta

Keywords:
Karonga
Geoarchaeology
Paleoecology
Micromorphology
Pedogenic carbonates
Middle Stone Age
Stable carbon and oxygen isotopes
Phytoliths
Pollen
Laterite

ABSTRACT

Mwanganda's Village (MGD) and Bruce (BRU) are two open-air site complexes in northern Malawi with deposits dating to between 15 and 58 thousand years ago (ka) and containing Middle Stone Age (MSA) lithic assemblages. The sites have been known since 1966 and 1965, respectively, but lacked chronometric and site formation data necessary for their interpretation. The area hosts a rich stone artifact record, eroding from and found within alluvial fan deposits exhibiting poor preservation of organic materials. Although this generally limits opportunities for site-based environmental reconstructions, MGD and BRU are located at the distal margins of the alluvial fan, where lacustrine lagoonal deposits were overprinted by a calcrete paleosol. This has created locally improved organic preservation and allowed us to obtain ecological data from pollen, phytoliths, and pedogenic carbonates, producing a regional- to site-scale environmental context for periods of site use and abandonment. Here, we integrate the ecological data into a detailed site formation history, based on field observations and micromorphology, supplemented by cathodoluminescence microscopy and μ-XRF. By comparing local, on-site environmental proxies with more regional indicators, we can better evaluate how MSA hunter-gatherers made decisions about the use of resources across the landscape. Our data indicate that while tree cover similar to modern miombo woodland and evergreen gallery forest prevailed at most times, MSA hunter-gatherers chose more locally open environments for activities that resulted in a lithic artifact record at multiple locations between 51 and 15 ka.

1. Introduction

Lithic artifact assemblages assigned to the Middle Stone Age

* Corresponding author. Institute for Archaeological Sciences and Senckenberg Centre for Human Evolution and Paleoenvironment, University of Tübingen, Tübingen, Germany.
E-mail address: fcschilt@ualg.pt (F. Schilt).

https://doi.org/10.1016/j.quascirev.2022.107638

(MSA) are found in Africa from ~315 to 20 thousand years ago (ka) and are associated with an increase in technological complexity among hunter-gatherers, as well as developments in abstract thinking and symbolism (Richter et al., 2017; Brooks et al., 2018; Scerri et al., 2018). At present, most of the MSA archaeological record comes from northern Africa, the northern part of the East African Rift Valley, and southern Africa (Mackay et al., 2014; Wadley, 2015; Scerri, 2017; Tryon, 2019). Malawi is situated in the important connecting region between the latter two regions (Mercader et al., 2009a; Bicho et al., 2016; Thompson et al., 2018).

The physical environment played a significant role in shaping human adaptation in eastern-central Africa, both regionally and locally (Basell, 2008; Kandel et al., 2016; Patalano et al., 2021). The choice of hunter-gatherers to use certain places was influenced by local conditions of resource availability (Kandel et al., 2016). However, most environmental records derive from large, basin-wide datasets, which cannot be linked directly to archaeological sites and human occupation (Cohen et al., 2007; Scholz et al., 2007; Scholz et al., 2011; Lyons et al., 2015; Ivory et al., 2018; Thompson et al., 2021b). In northern Malawi, paleoenvironmental research has focused on the study of sediment cores from Lake Malawi, dating back to 1.3 million years ago (Scholz et al. 2006, 2011; Cohen et al., 2007; Beuning et al., 2011; Lyons et al., 2015). These studies show that lakeshores transgressed and regressed hundreds of meters in elevation through time, and that there were extreme arid periods of near desiccation of the lake (Lyons et al., 2015). After 85 ka, lake levels remained relatively high, which has been attributed to more stable, wetter conditions caused by a shift in the position of the Intertropical Convergence Zone related to changes in orbital obliquity, eccentricity and precession (Ivory et al., 2016). This may be a major reason why the region developed an abundant MSA record after this time (Thompson et al., 2021b), but it does not explain how MSA people selected their activity areas across that landscape.

Previous studies showed that MSA sites in northern Malawi became more abundant after 75 ka within the context of the expansion of miombo woodland and mosaic savanna (Thompson et al., 2021a). Complicating interpretations, though, is the fact that most archaeological sites are found in alluvial fan deposits with thick lateritic soils (also known as Oxisols or Ferralsols), inhibiting the preservation of organic materials. These soils formed during periods of stability, overprinting the sedimentary layers created by the alluvial fan (Wright et al., 2017). Subsequent bioturbation and chemical weathering in laterites have homogenized deposits, erasing structural sedimentologic features, as well as former land surfaces (Wright et al., 2017). This confounds a clear understanding of local-scale environments in which MSA people concentrated their activities, and how these relate to different kinds of artifact production.

Mwanganda's Village (MGD) and Bruce (BRU) are two MSA sites located at the margins of the alluvial fan system to the west of Lake Malawi (Fig. 1). Overviews of artifact assemblages, fossils (in the case of MGD), and macro-scale geoarchaeological observations were previously reported from both sites (Clark et al. 1970, 1973; Clark and Haynes, 1970; Kaufulu, 1990; Wright et al., 2014). However, these studies lack essential data on timing and context of the artifacts.

With our work, we have taken advantage of the location of these neighboring sites on the distal part of the fan (Fig. 1) to access alluvial fan sediments as well as lake-lagoon deposits and paleosols. Combining geoarchaeological, paleoenvironmental, and chronological data, this paper aims to (1) investigate past environments, (2) achieve detailed reconstructions of site formation, and (3) place late MSA occurrences in a regional-to site-scale environmental context to address aspects of MSA forager behavior.

1.1. Geologic setting

The sites are located in the southern branch of the East African Rift System, which runs NNW-SSE and forms Lake Malawi (also known as Lake Nyasa or Lago Niassa), a large extensional graben lake. The down-faulted rift valley is bounded to the east and west by mountain ranges (Ring et al., 1992; Ring and Betzler, 1995). The underlying Malawi Basement consists mainly of gneisses and granulites of Precambrian to lower Paleozoic age. These metamorphic rocks are covered with Permian to Lower Jurassic volcanic and sedimentary formations of the Karoo system. Locally, the metamorphic Basement Complex and Karoo sediments are overlain by Early Cretaceous Dinosaur Beds consisting of friable sandstones, sandy marls, and clays (Betzler and Ring, 1995). The Chiwondo Beds unconformably overlie the Dinosaur Beds and have been temporally attributed to the Late Pliocene and Early Pleistocene based on biostratigraphy (Dixey, 1927; Stephens, 1963; Clark et al., 1966; Bromage et al., 1995), although they may extend into the early Middle Pleistocene (Kullmer, 2008). The Chiwondo Beds mainly consist of sandstones and siltstones of lacustrine origin, which have been deeply incised (Stephens, 1963) and are unconformably overlain by the Chitimwe Beds. The latter consist of eroded remnants of an extensive alluvial fan system, which drained into the lake (Fig. S1; Appendix A).

The Chitimwe Beds have long been recognized as hosting an abundance of MSA and LSA lithic artifacts (Dixey, 1930; Clark, 1966; Thompson et al., 2012; Wright et al., 2017; Nightingale et al., 2019). The alluvial fans originate from periodic erosion of the upland catchment of the western Rift shoulder where colluvium and weathering bedrock produce new sediments, which aggrade in lowland areas (Blair and McPherson, 1994). The movement and transport of catchment sediment depends on water input, gravity, vegetation, and mass wasting, and is especially promoted by flood conditions, which are common in Malawi between November and March due to monsoon-driven rainfall. Thompson et al. (2021b) have further suggested that human use of fire starting ~90 ka cleared tree cover to such an extent that it accelerated alluvial fan formation. Secondary processes modifying the sands and gravels of the Chitimwe Beds include surficial reworking by water and winnowing, as well as intensive weathering and laterite formation (Blair and McPherson, 1994; Wright et al., 2017). In the Karonga area, lateritic soil formation is widespread and likely induced by increased exposure of the soil to extremes in temperature and humidity after clearance of the forest cover (McFarlane, 1976). Agriculture and construction activities have increased erosion of alluvial fan deposits in many places, exposing numerous lithic artifacts.

1.2. Archaeological context

The Malawi Earlier-Middle Stone Age Project (MEMSAP) has taken a landscape approach to build a sequence of regional MSA behaviors and environments that would not be possible at a single locality. This has included survey (Thompson et al., 2014), geological and archaeological test pitting (Thompson et al., 2018; Thompson et al., 2021b), and more detailed archaeological excavations such as at MGD and BRU (Fig. 1) (Thompson et al., 2012; Thompson et al., 2022; Wright et al., 2014, 2017; Nightingale et al., 2019).

Unlike other detailed excavations in the area, which are located where Chitimwe Beds exhibit thick lateritic deposits (Wright et al., 2017), MGD and BRU are situated at the fringe of the alluvial fan. Both localities are situated on north-facing slopes overlooking the floodplain of the North Rukuru River, which drains into Lake Malawi ~7 km to the east (Fig. 1). Archaeological excavations in all

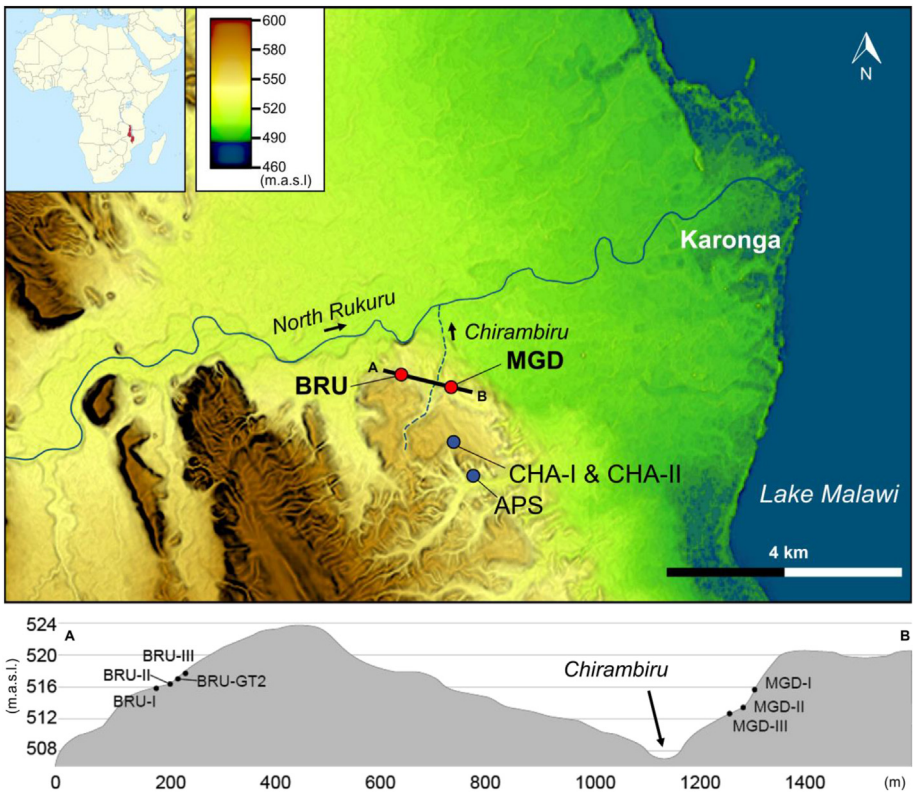

Fig. 1. Map of the area west of Karonga town indicating the site locations of Bruce (BRU) and Mwanganda's Village (MGD) on the hill slopes facing the catchment area of the North Rukuru River, which drains into Lake Malawi to the east (map produced with AW3D30 data). Modern lake-lagoons are visible as blue areas along the shore. Other published localities are indicated with blue dots: Airport Site (APS), Chaminade-I (CHA-I), and Chaminade-II (CHA-II). Below the map the modern topography is shown on a transect line between BRU and MGD (A, B) with the incision of the Chirambiru seasonal stream indicated in between the site areas. (For interpretation of the references to color in this figure legend, the reader is referred to the Web version of this article.)

trenches exposed MSA artifacts, but only two of them, MGD Area I and BRU Area II (Fig. 2), yielded assemblages in primary or close to primary context as demonstrated by refitting lithic artifacts (Wright et al., 2014). Likely in situ lithic artifacts were also uncovered from two additional tests pits at BRU (BRU-TP20 and BRU-TP21). The analysis of all these lithic materials is currently underway.

1.2.1. Mwanganda's Village (MGD)

In 1966, J. Desmond Clark led excavations at MGD, which had skeletal remains of an elephant, too fragmentary to assign to a genus, with artifacts scattered around the bones. He inferred that MGD was an ancient elephant butchery site associated with Sangoan tools, a type of artifact thought to occur in the earlier part of the MSA (Clark and Haynes, 1970). Later, Kaufulu (1990) reinvestigated the site with large geological trenches to further understand the relationship between the Chitimwe and Chiwondo Beds that were reported as occurring in contact at the location by Clark and Haynes (1970). This "Elephant Butchery Site" at MGD has since been frequently cited as an early MSA or Sangoan industry site with evidence for the in situ disarticulation of an elephant (e.g., Piperno and Tagliacozzo, 2001; Surovell and Waguespack, 2008; Yravedra et al., 2012). From 2009 to 2013, the Malawi Earlier-Middle Stone Age (MEMSAP) team mapped the area, collected samples, and conducted new excavations at MGD (MGD-I to III, Fig. 2). We conducted excavations adjacent to and upslope from the original elephant discovery location and dated the newly exposed sediments with Optically Stimulated Luminescence (OSL). We also examined the elephant remains for evidence of butchery, determined the age of elephant enamel fragments with Uranium–Thorium, and corrected maps from Kaufulu (1990), which show inaccurate positions of some of the geological trenches (Thompson et al., 2013; Wright et al., 2014). Based on these analyses, MEMSAP team members concluded that the fossils and artifacts were likely brought together through post-depositional processes (Wright et al., 2014).

Wright et al. (2014) distinguished four fluvial cut terraces across MGD dating to the Holocene, significantly post-dating MSA occupation. This terrace formation may be partially responsible for the mixing of sediments near the present-day surface but has not affected more deeply buried Pleistocene sediments. The excavation area at MGD-I (5 × 5 m) was positioned on a terrace uphill from Clark's trenches to obtain a longer sequence (Figs. 1 and 2). MGD-II (4 × 5 m) and MGD-III (4 × 5 m) were placed on a lower terrace next to Clark's excavations, with the purpose of re-examining the context of the "Elephant Butchery Site" (Figs. 2 and 3). A test pit located 13 m to the north and 10 m to the east of MGD-I showed a gravelly coarse sand deposit buried 1.7 m below the ground surface, which included artifacts and is bracketed by OSL ages between 43 ± 4 ka and 22 ± 2 ka (Wright et al., 2014). At MGD-I, unweathered lithic artifacts were found just above sediments dating to 26 ± 1 ka. These lithics, in this paper referred to as "classic" MSA, are typical of the Karonga MSA and comprise mostly casual and radial core reduction with little standardization of form and almost no retouch, but with some Levallois flake production and including flakes with large, faceted platforms (Thompson et al., 2018). Above this, terminal MSA lithics with multiple refits were recovered from sediments dating to between 26 ± 1 ka and 15 ± 1 ka (Thompson et al., 2021b). The terminal MSA assemblage displays both MSA and Later Stone Age (LSA) approaches to artifact reduction on the

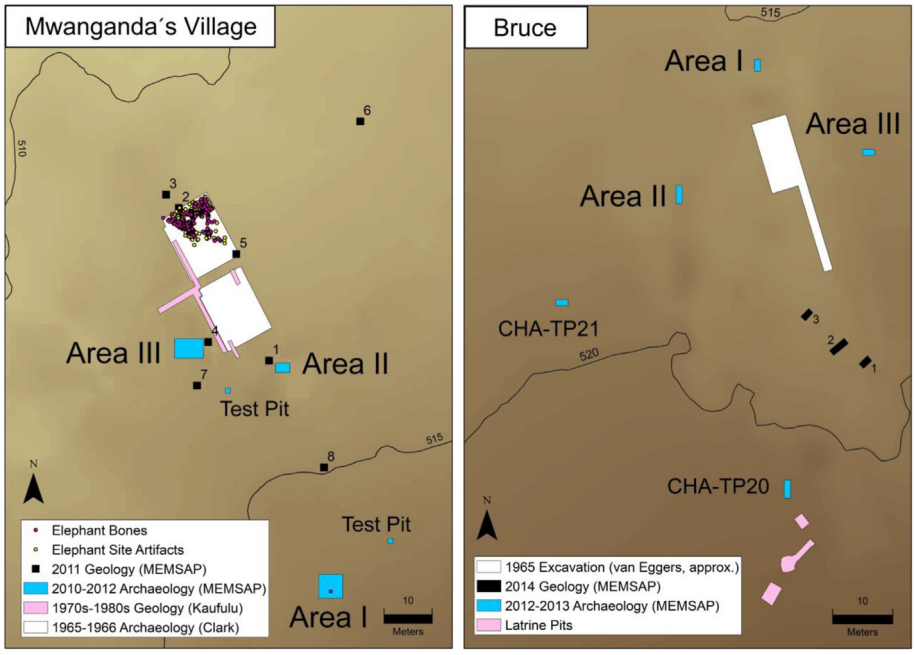

Fig. 2. Overview maps showing excavation areas of Clark and colleagues, Kaufulu, and MEMSAP at Mwanganda's Village (left) and Bruce (right). Darker browns are higher elevations, contour elevations are in m. The original designations for the two test pits at BRU were CHA-TP20 and CHA-TP21, as they were part of a larger survey program starting in the general area of Chaminade Secondary School (near CHA-I and CHA-II, Fig. 1). Here and in the text, they will be referred to as BRU-TP20 and BRU-TP21 for clarity.

same objects, e.g., a centripetal reduction strategy on small (2–4 cm) quartz pebbles rather than larger quartzite cobbles, resulting in pyramidal cores with neither final preferential detachments nor evidence for microlith production. This sequence supports an interpretation of the site as a place where people with varying MSA technological approaches returned multiple times, potentially over the course of ~10,000 years (Fig. 3).

1.2.2. Bruce (BRU)

In 1965, one of Clark's doctoral students, Alan van Eggers, supervised excavations at a site called Chaminade 1A, about 1 km northwest of MGD (Fig. 1). Although this was not described as a Sangoan site, there is a core-axe illustrated by Clark et al. (1970), alongside "classic" MSA artifacts such as Levallois points. Clark et al. (1970, 1973) also report pigments, which are absent at MGD, suggesting variation in activities carried out between the two sites. Through systematic test-pitting, local knowledge, and analysis of archive documents, MEMSAP identified a locality named BRU, later determined to be equivalent to Chaminade 1A. The high density of lithic artifacts and the presence of worked ochre on the surface also match the description in Clark et al. (1973). Although we are confident it is the same locality, unlike at MGD, we could not identify the exact location of the original excavation led by van Eggers relative to our new excavations. We therefore continue to use the MEMSAP designation BRU for the site.

Three archaeological excavation areas of 1 × 2 m (BRU-I to III), two archaeological test pits (BRU-TP20 and BRU-TP21), and three geo-trenches (BRU-GT1 to 3) were placed on the hillslope (Fig. 2). Beside the archaeological excavations and test pits, one of the geo-trenches, BRU-GT2, is included in this paper, as it exposed thick lagoonal deposits not well-represented in the archaeological excavations. Numerous lithic artifacts occur on the ground surface at BRU due to water erosion, which is especially active at this location due to agricultural activity and house construction. Although lithic assemblages were not stratified in a single pit but were exposed in several small excavations, the area shows repeated human occupation over many thousands of years. At BRU-II, unweathered artifacts occur in deposits dating between 34 ± 3 and 33 ± 3 ka, while at BRU-TP20 numerous concentrations of artifacts with some refits date between 51 ± 4 and 31 ± 2 ka (Thompson et al., 2021b). Bedrock was not reached in any of the excavations.

2. Methods

The primary methods of analysis involved micromorphological study of block sediment samples and carbonate nodules, palynology, phytolith analysis, and the analysis of stable isotopes from pedogenic carbonates. In this paper we also report two new OSL ages from BRU-TP21. Methods are summarized in this section; additional information is provided in the supplementary material (Chapter S1; Appendix A).

2.1. Field descriptions

All exposed sections were described following the "USDA Field Book for Describing and Sampling Soils" (Schoeneberger et al., 2012). Visual observations were aided by a hand lens, and included for each sedimentary unit descriptions of texture, color, structure, weathering features, inclusions, carbonate content, consistency, clay films, disturbances, and unit boundaries. Colors on dry sediment were described using the Munsell soil-color charts (Color X-rite 2009). Feel tests and soil ribbon tests were regularly performed when textures were loamy or clayey (Thien, 1979).

2.2. Micromorphology, cathodoluminescence, and microscopic X-ray fluorescence

Micromorphology was used to reconstruct site formation processes and served as a basis for other analyses and to guide subsample collection. 47 block samples and 15 carbonate nodule samples were collected from exposed profiles at MGD and BRU, producing 95 thin sections. Based on field observations and micromorphology, the sedimentary and pedogenic units of MGD and BRU were grouped into facies (Walther, 1894; Middleton, 1973).

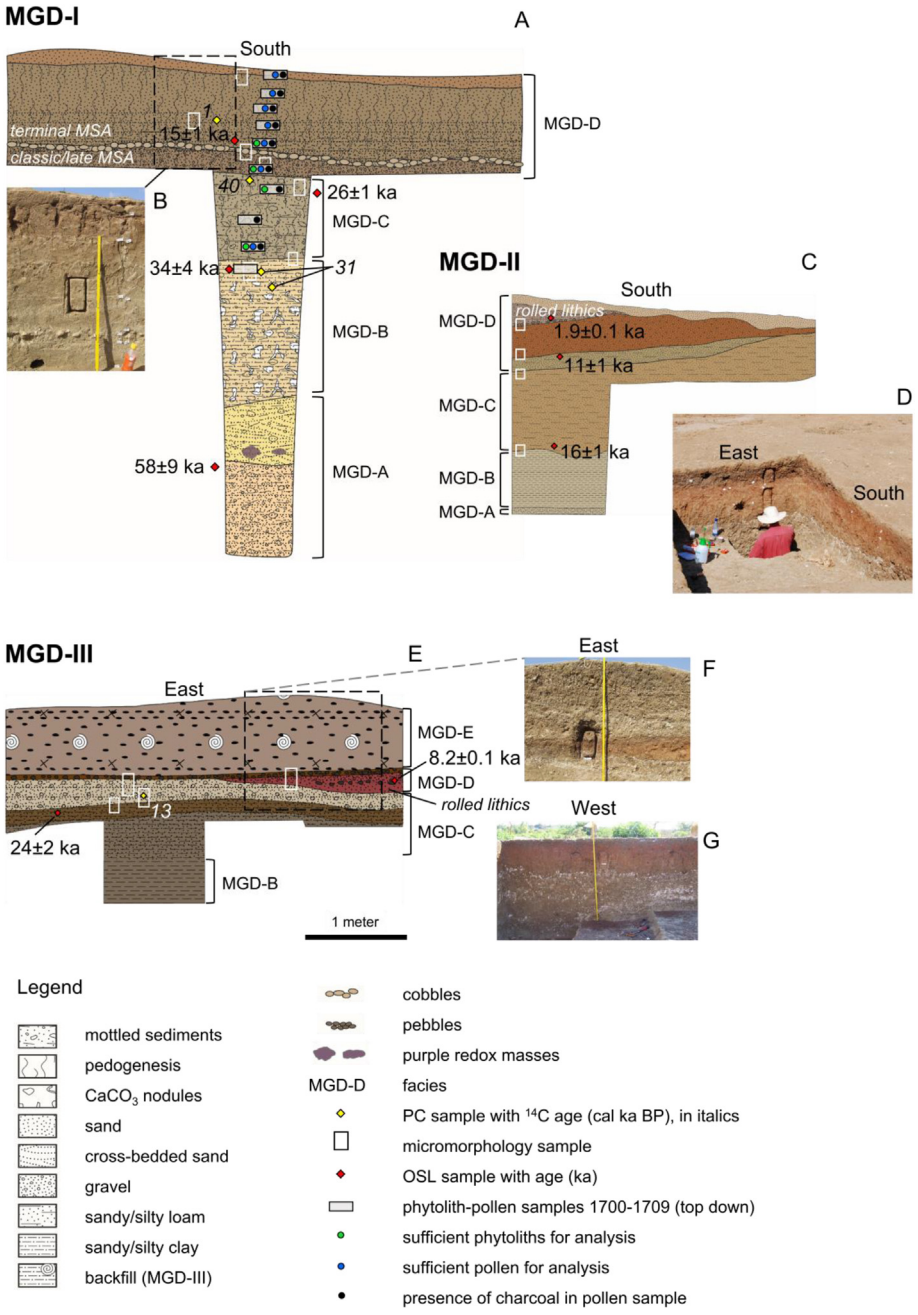

Fig. 3. Profile drawings of the excavation areas at MGD. At MGD-I (A), late "classic" MSA lithic artifacts were recovered from below the cobble layer within facies *MGD-D*, and terminal MSA artifacts were found above the cobble horizon. The inset photo B shows facies *MGD-D* with a partly carved out micromorphology sample, and an empty termite fungus chamber in the lower left. The modern soil rubifies towards the top. The inset photo D shows the East and South profiles of MGD-II during sample collection. Photo F shows shallow channel fill deposits (orange red) in the East profile of MGD-III, which are overlain by a thick overburden from the historic excavations, appearing whitish gray as it contains carbonate nodules and clay from facies deriving from *MGD-B* and *MGD-C*. Inset photo G was taken from the opposite side, presenting a stratigraphic sequence without overburden deposits. A reddish deposit of coarse sand and gravel (equivalent to the shallow channel fill in the West profile) is infilling a channel incision cutting into facies *MGD-B* and *MGD-C*. The sequence is topped by a thin stony, organic-rich, horizon of winnowed cobbles and pebbles. OSL dates (ka) are displayed in roman typeface and radiocarbon dates on pedogenic carbonates are shown in italics (cal ka BP) and have been calibrated in OxCal v.4.4 (Ramsey et al., 2013) using the SHCal20 atmospheric curve (Hogg et al., 2020). The sediments and soils were grouped into facies, which are described in the results section. (For interpretation of the references to color in this figure legend, the reader is referred to the Web version of this article.)

In addition to the analysis with stereoscopic and petrographic microscopes, we used a cathodoluminescence (CL) microscope on a selection of thin sections. Observations were recorded with photomicrographs (Chapter S5; Appendix A). Microscopic X-ray fluorescence (μ-XRF) was used to determine relative abundances of major and trace elements (Mentzer and Quade, 2013), and was performed on a selection of samples (Chapter S6; Appendix A).

2.3. Paleoecology

Pollen and phytolith samples were collected in the field as bulk sediment samples from exposed profiles. The profiles were first cleaned from top to bottom with a hard brush to remove loose sediments and sampled from bottom to top with a trowel and dustpan. The trowel and dustpan were cleaned in soapy water and

rinsed in plain water followed by thorough air drying between sampling episodes.

2.3.1. Palynology

Palynology was attempted only at MGD (Fig. 3). Ten sediment samples were processed for pollen and micro-charcoal (particles <125 μm) analyses, following the methods described in Moss (2013). Seven of the samples contained pollen (1700–1705, and 1708) with concentrations between 200 and 700 grains per cm^3. Nine of the samples contained charcoal (1700–1708).

2.3.2. Phytolith analysis

The nomenclature for phytolith classification used in this paper follows Madella et al. (2005). Supporting keys from pertinent regions include: Runge (1999); Fahmy (2008); Albert et al. (2009); Barboni and Bremond (2009); Neumann et al. (2009), Neumann et al. (2017); Eichhorn et al. (2010); Novello et al. (2012); Albert et al. (2015); Collura and Neumann (2017), as well as past phytolith work on referentials and archaeological localities from both the Malawi side of the lake (Wright et al., 2017; Nightingale et al., 2019; Thompson et al., 2021b) and the Mozambican shore (Mercader et al., 2009b; Mercader et al., 2010; Mercader et al., 2011).

2.3.3. Stable isotope analysis ($\delta^{13}C_{PC}$ and $\delta^{18}O_{PC}$)

Stable isotopes from pedogenic carbonates ($\delta^{13}C_{PC}$, $\delta^{18}O_{PC}$) were measured to reconstruct aspects of vegetation and climate during soil formation (Cerling, 1984). The analyses were performed on 27 sub-samples from 18 pedogenic carbonate nodules. The samples were calibrated against the NBS 18 standard: $\delta^{13}C = -5.014‰$ and $\delta^{18}O = -23.2‰$. All $\delta^{13}C_{PC}$ and $\delta^{18}O_{PC}$ measurements are expressed in permille (‰) in relation to the Vienna Peedee Belemnite (VPDB) standard.

2.4. OSL dating

OSL ages on quartz grains from two samples (LM13-10, LM13-11) collected at BRU-TP21 were determined by protocols similar to Wright et al. (2017), using small aliquots (~3 mm mask size), consisting of several hundreds of quartz grains (180–212 μm in diameter). OSL measurements were carried out using a Risø TL/OSL reader (Model TL/OSL-DA-20C/D) at the Korea Basic Science Institute. Burial equivalent doses were calculated using the Single Aliquot Regenerative dose (SAR) procedure. Dose rate estimations were determined by low level high resolution gamma spectrometer. The resulting ages are included in Table 2, and more details are reported in the supplementary material (Table S6, Fig. S2, and Fig. S3; Appendix A). Other ages referred to in this paper have been previously published in Thompson et al. (2018) and Thompson et al. (2021b).

3. Results

3.1. Lithostratigraphy of MGD and BRU— key field and micromorphological observations

For a complete overview of the units, we refer to the supplementary material (Table S12, Table S13; Appendix A). A schematic overview of the profiles of the archaeological excavations and their facies is given in Fig. 5. The facies are further summarized and contextualized with the ecological data, chronology, and archaeology

Table 1
Facies at MGD from top to bottom with OSL ages (ka) of the deposits at each site area ("Area"), radiocarbon dates (cal ka BP) on pedogenic carbonates (PC), brief descriptions of sediments, ecological data, interpretation, and archaeology. All radiocarbon ages reported here and referenced in the text were calibrated in OxCal v.4.4 (Ramsey et al., 2013) using the SHCal20 atmospheric curve (Hogg et al., 2020). *The shallow *MGD-D* channel fill deposits at MGD-II and MGD-III date to the Holocene, while the deeper artifact bearing deposits at MGD-I are Late Pleistocene and preserve a segment of sediments lacking at the other site areas.

Facies	Area	OSL (ka)	$^{14}C_{PC}$ (cal ka BP)	Description	Pollen	Charcoal	Phytoliths	$\delta^{13}C_{PC}$ (‰)	Interpretation	Archaeology
MGD-E	III	–	–	Laminated silty clay, $CaCO_3$ nodules with inclusions of yellow clay coatings	N/A	N/A	N/A	N/A	Overburden from previous excavations	Reworked
			«Clear to abrupt boundary»					*«(Historic) ground surface»*		
MGD-D	I	15±1*	1	Coarse textures ranging from very coarse sands to very coarse gravels, cobbles & sandy loam	Dominated by grasses, with reeds, evergreens	Abundant in the top. Declining downward	Morphologies closest to referentials of gallery forest & woodland	−9.7	Riverbed & mass-wasting deposits containing reworked soil & sediment.	Sharp-edged "classic"/late MSA & terminal MSA with conjoins
	II	11±1–1.9±0.1*	–						Stream channel fill & mass-wasting deposits containing reworked soil & sediment	Rolled lithics
	III	8.2±0.1*	–							
			«Abrupt boundary»						*«Erosional contact»*	
MGD-C	I	26±1–16±1	–	Coarse to very coarse sandy loam, abundant secondary carbonates	Generally higher proportion of aquatic taxa	Present in all samples	Morphologies most common in trees & bushes	−7.6	Wooded seasonal wetland. Paleosol in mixed fluvial & lagoonal deposit with pedogenic carbonates indicating gradual increase of dry surface conditions	Locally, rolled. Bones & lithic artifacts in the top 10 cm of this facies at Clark's Elephant Butchery Site
	II	–	–							
	III	–	13							
MGD-B	I	34±4 (top)	31-30, 40	Laminated silty clay with secondary carbonates	Not preserved	Not preserved	Not preserved	−10.8 to −10.1	Lake-lagoon	None
	II	–	–							
	III	–	–							
MGD-A	I	58±9	–	Pale colored bedded angular medium to coarse sands & fine gravel	N/A	N/A	N/A	N/A	Stream deposits in the distal part of the alluvial fan, Chitimwe Beds	None
	II	–	–							

Table 2
Facies at BRU from top to bottom with OSL ages of the deposits at each site area ("Area"), radiocarbon dates on pedogenic carbonates (PC), brief descriptions of sediments, interpretation, and archaeology. The sediments at Bruce did not yield enough phytoliths for analysis and pollen analysis was not attempted. The complete radiocarbon and OSL dates including the new ages for BRU-TP21 can be found in the supplementary material (Table S4, Table S5, and Table S6; Appendix A) and Thompson et al. (2021b).

Facies	Area	OSL (ka)	$^{14}C_{PC}$ (cal ka BP)	$\delta^{13}C_{PC}$ (‰)	Description	Interpretation	Archaeology
BRU-D	GT2	–	–	N/A	Coarse sand to medium gravel	Recent channel fill	–
			«Clear erosional break between BRU-D & BRU-A (observed at BRU-GT2)»				
BRU-C	I	54±5–29±3	–	N/A	Beds of imbricated medium sands to medium gravels. Sandy clay & loamy sand in the lowest units. Mineral weathering, in situ silt & clay formation. Redox depletions & concentration in lower units	Distal part of the alluvial fan, defined by gullying & stream bed deposition. Chitimwe Beds.	Many "classic" MSA lithic artifacts, ochre fragments
	II	–	–				
	III	–	–				
	TP20	51±4–31±2	–				
	TP21	39±2–20±1	–				
BRU-B	III	>41±5	29–20	−10.9 to −8.8	Silty clay with 10–15% coarse sand to fine gravel	Nodular calcrete in sediment mixed by soil cracking & bioturbation	Few lithic artifacts
BRU-A	GT2	–	33–28	−9.2 to −7.6	Silty clay with few very fine sand inclusions, decomposing organic matter & large carbonate nodules	Lagoon, overprinted by wetland soil with palustrine carbonate nodules	–
	III	–	–	–			

in Table 1 for MGD, and in Table 2 for BRU. More detailed field and micromorphological descriptions, CL-microscopy, and μ-XRF results can be found in the supplementary material (Chapters S4, S5, and S6, respectively; Appendix A).

3.1.1. Mwanganda's Village

The stratigraphy at MGD shows some variability between the site areas as a result of their positions on different parts of the slope. The facies comprise in detail, from oldest to youngest:

3.1.1.1. MGD-A. The lowermost facies, *MGD-A*, consists of angular coarse sands and fine gravel with 1–2% coarse rounded pebbles. Clear horizontal depositional planes and crossbedding are preserved. The facies is grayish white to yellowish in color with faint, dm-scale yellow and purple redox masses (Fig. 3).

3.1.1.2. MGD-B. This facies formed under non-turbid, subaqueous conditions which involved the deposition of silty clay as suspended load with intercalated laminations of fine sand. The clay is rich in mica, giving it a greenish color (Fig. 6a). Carbonate nodules are common in this facies and vary in size from 1 mm to ~15 cm. Inclusions of organic remains inside the nodules and the occurrence of both alpha-type microfabrics (formed by physical and chemical processes) and beta-type microfabrics (formed by biogenic processes) within the nodules are indicative of palustrine-pedogenic formation (Wright, 1990a; Alonso-Zarza and Wright, 2010a). Because the finely laminated deposit is well-structured, bioturbation features appear very distinct (Fig. 6a). They mainly consist of chambers (1–2 cm in diameter), interconnected by a network of channels. Towards the top, an increase in bioturbation by soil fauna, desiccation cracks and root disturbances is observed.

3.1.1.3. MGD-C. MGD-C is a welded, buried paleosol, corresponding to the paleosol described by Clark and Haynes (1970), the top 10 cm of which was the context of the elephant bones and lithic artifacts. *MGD-C* initially formed in a lagoonal environment but was subsequently overprinted by soil formation and the admixture of coarse alluvial sediment through cracks and bioturbation, giving the facies a loamy texture (Fig. 6b, c, f, g). After this, a calcrete formed in the mixed sediments. *MGD-C* appeared massive in the field but in thin section, many mixing agents were distinguished, including shrink-swell within the soil, the formation and infilling of desiccation cracks, root action, bioturbation by soil fauna, and pedogenic carbonate formation. Their compounding effects obliterated potential pre-existing sedimentary structures (Fig. 6c, h, i, k). However, rare 1-3-cm sized angular and pillar-shaped peds of laminated clay (similar to facies *MGD-B*) were found in their original depositional orientation, revealing the sedimentary origin of the soil parent material (Fig. 6g). CL-microscopy of the pedogenic carbonate nodules has shown that both types of sediment have been replaced by carbonate, indicating that mixing of the lagoonal clay with alluvial deposits occurred well before the paleosol became a mature calcrete. Generally, the formation of nodular calcretes constitutes the final stage of soil development in this type of environment (Blokhuis et al., 1990). Clay coatings and reworked fragments of clay coatings are rare, but few intact and fragmented, laminated, limpid yellow clay coatings were observed near and inside carbonate nodules, some of which are partially dissolved and substituted by microsparitic carbonate (Fig. S10c; Appendix A).

3.1.1.4. MGD-D. This facies consists of fluvial and alluvial fan-related deposits, which overly *MGD-C* with an abrupt (0.5–2 cm) to clear (2–5 cm) boundary (sensu Schoeneberger et al., 2012). The sediments are coarse, ranging from fine-to very coarse sand and sandy loam, to very coarse gravels and cobbles. Sand-to fine gravel-sized materials are subangular to subrounded, while coarse gravels (pebbles) and cobbles are generally subrounded to rounded. At the site area located uphill, MGD-I, bedded fine gravels and a cobble layer were deposited directly on top of facies *MGD-C*, which have been overprinted by different episodes of soil formation involving the formation of a subangular blocky microstructure and thick, typic pale yellow dusty clay coatings with irregular laminations and deformations (Fig. 6j). This type of clay coating forms as a result of repeated cycles of wetting and drying with vertic activity (shrink-swell) and may form at shallow depths (Kühn et al., 2010). The overlying deposits are richer in clay (sandy loam) due to the inclusion of inherited materials from facies *MGD-B* and *MGD-C*, in particular weathered and rolled fragments of laminated clay peds and reworked carbonate nodules. In situ (orthic) carbonate features are rare or weakly developed compared to the two facies below and consist of biogenic, beta-type features such as micritic (crystal size <5 μm) hypocoatings, needle fiber calcite, and small micritic nodules, typical for the vadose zone (Wright, 1990a; Alonso-Zarza and Wright, 2010a). Clay coatings are common and become more

abundant towards the top where they exhibit pendant and crescent shapes typical for clay illuviation in a part of the soil where top-down soil processes are dominating. They are distinct from the clay coatings in the fluvial deposits below, and indicative of improved drainage relative to the preceding depositional phase.

At MGD-II and MGD-III, facies *MGD-D* is defined by a paleo-channel incision (Fig. 3), which is infilled with reddish sediment of bedded sandy clay loam, dispersed cobbles, and gravels, which are strongly bioturbated (Fig. 6k). Shrink-and-swell activity is evidenced by grano- and poro-striated b-fabrics. Clay coatings and in situ carbonate features are rare. The red color of the sediment shows similarity to lateritic soils common in the Chitimwe alluvial fan deposits. The carbonate nodules present in some of the coarser channel fill sediments were likely redeposited from eroding parts of the paleosol of *MGD-C*, or from *MGD-B*. Needle fiber calcite has formed adjacent to some carbonate nodules, possibly in relation to dissolution and disintegration of the nodule edges. Common small (1–3 mm) Fe–Mn disorthic and orthic nodules can be found, indicative of weak lateritic soil formation (Marcelino et al., 2010). A thin, dark brown organic topsoil composed of pebbles in clay loam represents the historic ground surface. It directly overlies *MGD-C* in the northern part of MGD-III and caps the channel fill of *MGD-D* occupying the southeastern part of the excavation (Fig. 3).

3.1.1.5. MGD-E. *MGD-E* comprises the overburden (~50 cm) from Clark's old excavations covering the historic surface on the eastern part of MGD-III.

3.1.2. Bruce

The site areas at Bruce (BRU) contained four facies with 24 sedimentary units (Table S13; Appendix A). An overview of the facies is given in Table 2. Fig. 4 shows profiles of the three excavation areas and geo-trench BRU-GT2.

3.1.2.1. BRU-A. Facies *BRU-A* consists of white, fine carbonate silt and lagoonal deposits of laminated silty clay similar to facies *MGD-B*. It contains abundant large fragments of partly decomposed organic matter.

3.1.2.2. BRU-B. This facies was exposed at BRU-III and is represented by a welded calcrete paleosol similar to *MGD-C*, with coarse sand introduced by bioturbation and soil cracking. Many siliceous minerals, deriving from both the lagoonal clay and the alluvial fan deposits, have been (partly) dissolved and gradually replaced by carbonate (Fig. 7a–h). Petrography and CL-microscopy reveal the primary source material as reflected in the shapes of pseudomorphic pore spaces after dissolved minerals, calcite replacement of dissolved siliceous grains, and sparitic neoformation around the edges of sand grains affected by dissolution (Fig. 7g and h). This process is better visible in *BRU-B* than in *MGD-C*, which may be attributed to a less advanced level of maturity reached by the calcrete at BRU compared to MGD, although both fall in the same calcrete category (stage 3), following Machette (1985).

3.1.2.3. BRU-C. *BRU-C* comprises artifact-bearing, lateritic sands

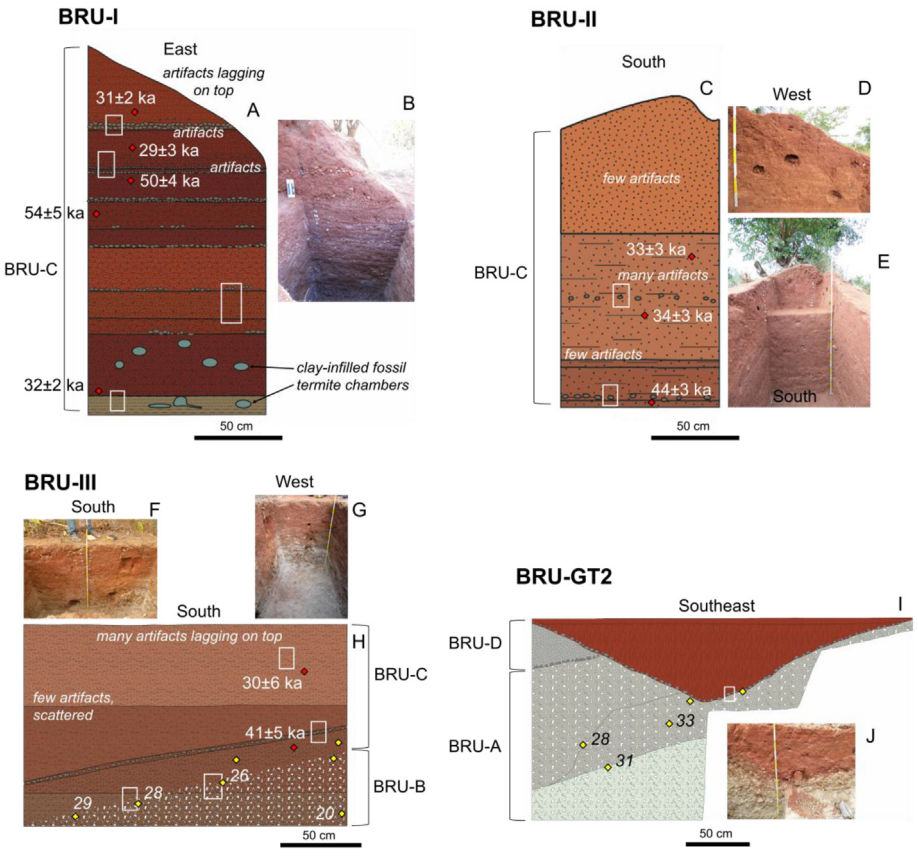

Fig. 4. Profile drawings of the three excavation areas (BRU-I, BRU-II, BRU-III) and a geo-trench (BRU-GT2) at BRU, displaying sample locations for micromorphology (rectangles), pedogenic carbonate nodules (yellow diamonds), OSL ages (in roman) and radiocarbon dates (cal ka BP, in italics) from selected pedogenic carbonate nodules. For the legend, see Fig. 3. The sediments and soils were grouped into facies, which are detailed in the results section. One of the facies (*BRU-B*, found at BRU-III) is defined by calcrete soil formation. Different from the similar paleosol horizon of facies *MGD-C*, there are no signs that *BRU-B* was truncated and the soil horizon with pedogenic carbonates formed after burial by *BRU-C*. Consequently, sediments of *BRU-C* are older than the paleosol they cover. The top of BRU-II consists of a biomantle with abandoned termite chambers, as can be seen on the inset photo (D). (For interpretation of the references to color in this figure legend, the reader is referred to the Web version of this article.)

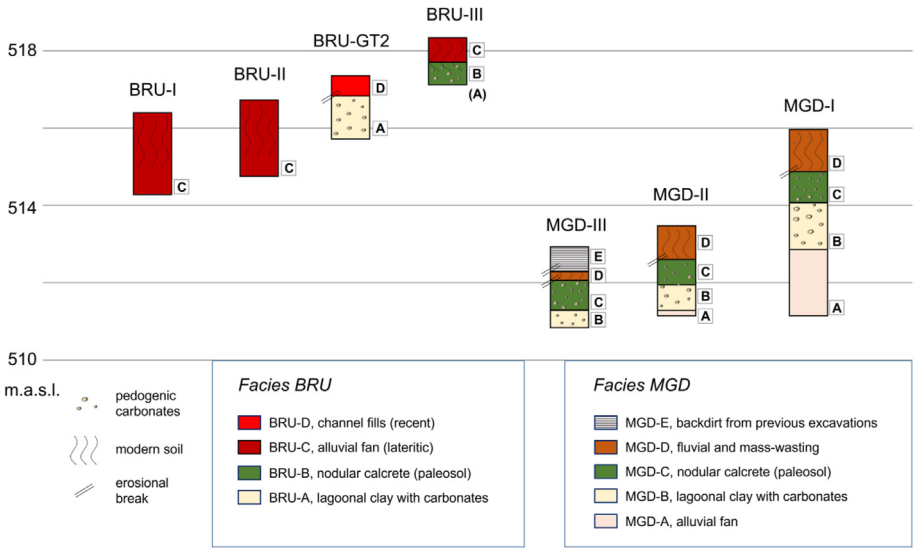

Fig. 5. Overview of four trenches at BRU (left) and three at MGD (right) along a NW-SE transect indicating the different facies within each profile. The y-axis indicates elevation in meters above sea level (m.a.s.l.), based on AW3D30 data (see transect in Fig. 1). At BRU-III, facies *BRU-A* was only observed at the bottom of the pit and is therefore indicated between brackets. Facies *BRU-A* is equivalent to *MGD-B*, and carbonate paleosols developed in *BRU-B* and *MGD-C* but extend with palustrine-pedogenic carbonates into the underlying facies *BRU-A* and *MGD-B*. The excavation areas are arranged from west to east, but the x-axis of the figure does not reflect accurate distances (refer to Fig. 1).

and gravels, which formed mainly by gullying, stream deposition, debris flow, and winnowing. Sand and very fine gravel-sized grains are subangular to subrounded, while fine to medium gravel is generally subrounded to well-rounded. The deposits vary between the site areas and include breaks in sedimentation likely associated with numerous erosional events. However, OSL dates the excavated deposits to between 29 ± 3 and 54 ± 5 and soil formation and confirms the temporal constraint of depositional processes at BRU. Lateritic soil formation with mineral weathering impacted the sediments considerably at all site areas. A multi-step weathering sequence could be observed, beginning with the disintegration of larger fragments (sand, gravel) and the formation of authigenic (silty) clay (Fig. 7j and k), followed by its vertical translocation, and ending with the formation of limpid, finely laminated clay coatings (Fig. 7l, m, n, o). Indications for erosional processes within the soil were observed at BRU-I (Fig. S16; Appendix A). As opposed to *MGD-D*, *BRU-C* deposits do not contain inherited soil materials, suggesting that the calcrete (*BRU-B*) was not truncated at the Bruce site location.

3.1.2.4. BRU-D. This facies consists of relatively recent channel fill with clast-supported, very coarse sand to fine gravel.

3.2. Paleoecology

3.2.1. Pollen

Facies *MGD-D* contained pollen from six consecutive samples (samples 1700–1705), and the lowermost (1708) sample from *MGD-C* yielded enough pollen for analysis as well (Fig. 8). Overall, the pollen record was dominated by herbs, especially grass (30–40% of the pollen sum), of which aquatic taxa, in particular sedge, formed the next most important group, and arboreal taxa (montane forest, evergreen forest, and woodland) making up between 10 and 15% of the pollen sum. Pteridophytes were also present in samples 1702 to 1705 and 1708. In terms of general trends with changes in pollen taxa there is a clear transition from samples 1705 to 1703 and 1702 to 1700, with a decline in woodland taxa (particularly *Blighia* sp. and Asteraceae) and an increase in Brassicaceae and *Eucalyptus* sp. Charcoal values are generally around 200,000 particles per cm^3, except for samples 1709 (no charcoal present), 1707 (<100,000 particles per cm^3), 1701 (<50,000 particles per cm^3) and 1700 (~400,000 particles per cm^3).

3.2.2. Phytoliths

The total number of phytoliths tallied for the current study is 1077 from 12 samples, seven of them coming from MGD-I (tally of 908) and five from BRU-TP20 (Table S7; Appendix A). Their respective phytolith records vary, with low counts (n = 0–31) for BRU-TP20 and for samples 1703, 1707, and 1709 from MGD-I (Fig. 3), which were thus excluded from further analysis and paleoenvironmental interpretation. For the productive samples from MGD-I, phytolith weathering/dissolution affects a very minor part of the assemblage: <2%. Morphotype diversity is somewhat limited, totaling 33 discrete shapes. Mean morphotype frequency is ~6 (range = 1–556). Five morphotypes are very common, representing more than 85% of the total variability, and in numbers above the mean (n = 31–556). These morphotypes are, in order of dominance: 1) globular granulate (~53% from the total), 2) blocky (~14%), 3) cylindroid psilate (~10%), 4) tabular elongate (~6%), and 5) bilobate short cells (~6%), with the remainder of the assemblage representing 11% of the total phytolith count (Fig. S5; Appendix A).

Archaeological phytolith assemblages from MGD-I follow a non-normal distribution. A Principal Components Analysis (PCA) transformed 12 variables (phytolith classes) into loading values upon standardization. Raw counts used for PCA are in the supplementary material (Table S8; Appendix A). The first and second components account for 61.32% of the variance. This PCA includes samples from MGD (Fig. 3), along with three comparative datasets representing the phytolith spectra from known modern local and regional environments, which represent various ecofacies within Zambezian woodlands (Mercader et al., 2011). The archaeological data processed for the PCA come from MGD-I (this paper), along with contemporaneous MSA sites in Mozambique (Mercader et al., 2013) and Tanzania (Mercader et al., 2021b) for comparison. The

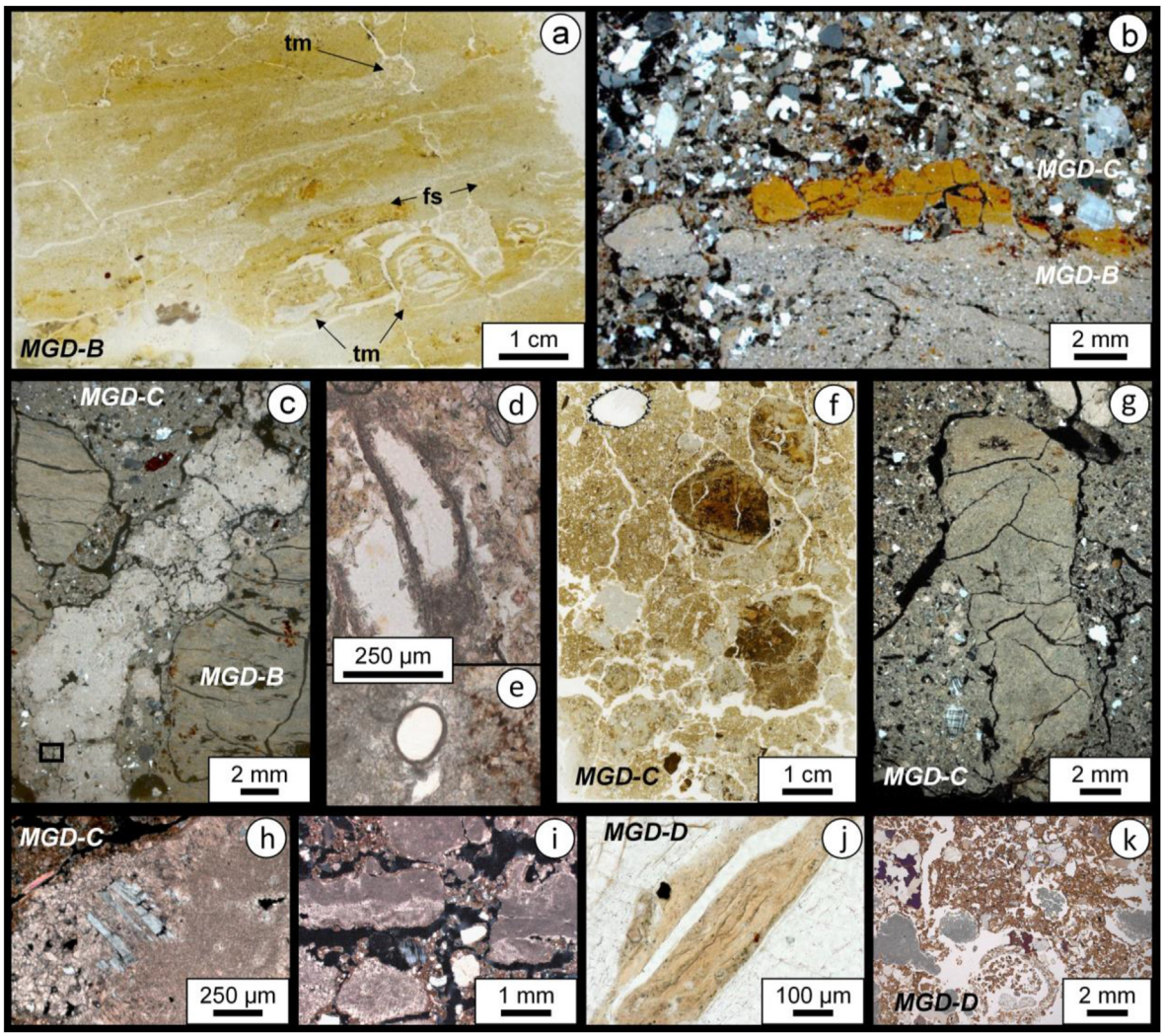

Fig. 6. Micromorphology of MGD. a) Thin section of silty clay with interbedded laminations of fine sand (fs) and termite features (tm). b) Boundary between intact clay in *MGD-B* and bioturbated *MGD-C*, showing contrasting grain sizes of *MGD-B* (silt, clay) and *MGD-C* (coarse sand, clay) and a fragmented orange slaking crust at the contact (XPL). c) Sandy loam infilling envelops a pedogenic carbonate nodule in a crack within facies *MGD-B* (XPL). d) and e) show calcified organic remains including a root fragment in a biogenic carbonate nodule shown in (c) (small black frame, PPL). f) Thin section from a part of *MGD-C* with organic remains and carbonate nodules. g) Pillar-shaped remnant of laminated silty clay in sandy matrix (XPL). h) Brecciated feldspar with dissolution voids and microsparite (~5–20 µm) (XPL). i) Flat blocky merging carbonate nodules with internal microlayers of different calcite crystal sizes (XPL). j) Deformed pale yellow dusty clay coatings (PPL). k) Vertical channel (upper left) leading to a circular termite feature in between carbonate nodules (gray) affected by dissolution (PPL). (For interpretation of the references to color in this figure legend, the reader is referred to the Web version of this article.)

PCA shows two clusters, which together represent a continuum of wooded and forested paleoenvironments (Fig. 9). Quadrant no. 2 clusters the Mozambican MSA sites with woodlands. Quadrant no. 4 groups all samples from MGD-I between a Zambezian gallery forest of Guineo-Congolian affinity and the mesic woodland reconstructed from the Nasera Industry site of Mumba in Tanzania (Mercader et al., 2021b). For contrast, we also included a hydromorphic grassland nested within a miombo woodland, locally known as a "*dambo*," noticing that all archaeological and reference samples plot far from this outlier.

3.2.3. Stable isotopes

The results of the carbon and oxygen stable isotope analysis of pedogenic carbonate nodules ($\delta^{13}C_{PC}$ and $\delta^{18}O_{PC}$) from MGD and BRU are represented in Fig. 10. $\delta^{13}C_{PC}$ VPDB values are between −10.9‰ (min) and −7.6‰ (max) (range of 3.2‰), with a mean value of −9.3‰ and a standard deviation of 1.1. $\delta^{18}O_{PC}$ VPDB values are between −9.1‰ (min) and −6.3‰ (max) (range of 2.8‰), with a mean value of −8.2‰ and a standard deviation of 0.5. The scatterplot further gives an overview of the facies from which the carbonate samples were collected, their age brackets, and the inferred wood cover associated with decreasing $\delta^{13}C_{PC}$ values. The complete results are provided in the supplementary material (Tables S1 and S3; Appendix A).

4. Discussion

4.1. Complications of OSL dating

All OSL dates are in stratigraphic order, except at BRU-I (Fig. 4). Out-of-order OSL ages are attributed to potential partial resetting of OSL signals in quartz during fan formation, soil formation processes and/or uncalculated errors in time-averaged water content in the different parts of the profile. Soils are dynamic environments as minerals undergoing secular equilibrium are mobile, which moves sources of ionizing radiation into new aspects of the profile over the time of formation. In addition, water attenuates the absorption of radiation in the crystal matrix of sedimentary minerals, but the

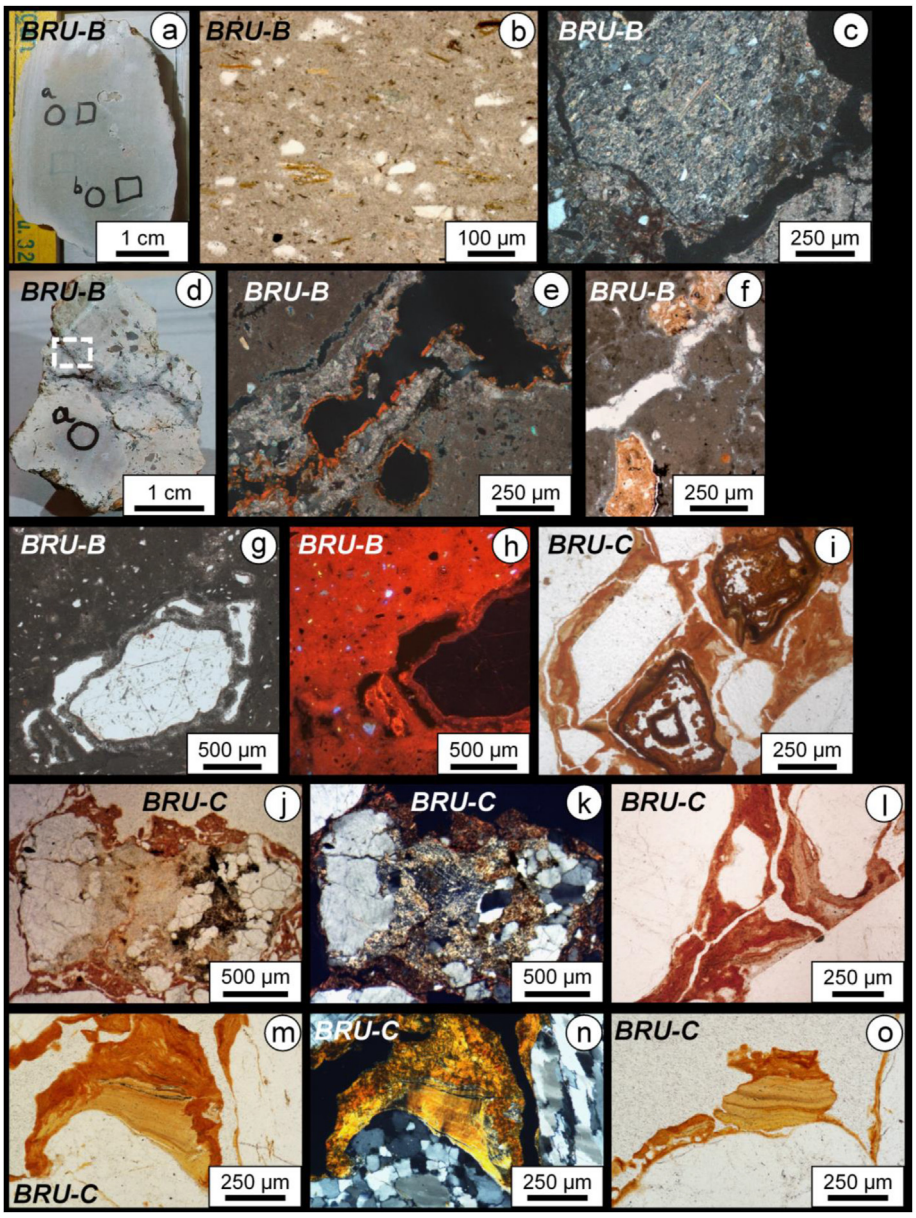

Fig. 7. Micromorphology of BRU. a) Carbonate nodule after laminated silty clay (*BRU-A*) of fine micrite. b) laminated mica inside a carbonate nodule (PPL). c) Tilted ped of laminated clay showing partial dissolution and calcite replacement (XPL). d) Carbonate nodule from the top of *BRU-B* with zones with sand inclusions and cracks with sparite infillings and clay coatings. e) Crack (black) with a sparite (light) coating starting to infill the crack, overlain by an orange limpid clay coating (rectangle in [d], XPL). f) Two inclusions of clay domains in a micritic nodule with an accommodating plane (fissure) partially infilled with sparite (PPL). g) Sand grain inside a carbonate nodule with multiple dissolution phases represented by void spaces and carbonate. Equivalent to the one displayed in (h) (PPL). h) Episodes of dissolution around a siliceous sand grain have been partially filled with sparitic (bright red) and micritic (darker red) calcite. Some silt in the surrounding micrite appears blue (quartz) or yellow (feldspar). Black specks may indicate pore spaces pseudomorphic after dissolved silt grains (CL). i) Ferruginous open boxworks of alteromorphs (Delvigne and Stoops, 1990) (PPL). j-k) In situ clay (yellowish, probably sericite) formation inside a heavily weathered feldspar pebble (j in PPL, k in XPL). l) Different phases of clay illuviation represented by coarse yellow to orange clay coatings (PPL). m-n) A yellow laminated clay coating has been truncated on the side and overprinted by dark orange coarser clay illuviation (m in PPL, n in XPL). o) Remnant clay coating on a sand grain, indicative of erosional processes within the soil (PPL). (For interpretation of the references to color in this figure legend, the reader is referred to the Web version of this article.)

relative content of water mass over the duration of burial can be variable, particularly in open environments, and therefore is a common source of uncertainty in OSL dating (Diaz et al., 2016). Other bioturbation effects such as termite and root disturbance can affect grain distributions over the course of millennia (Kristensen et al., 2015). At BRU-I, termite activity was likely the main cause for out-of-order OSL ages in the lower part of the profile, as evidenced by clay-infilled fossil termite chambers (Fig. 4). This does not affect the dating of the archaeological occurrences at this site area, which came from less bioturbated overlying deposits, or our paleoenvironmental reconstructions, which are based on samples collected from other profiles.

4.2. Soils: laterites and welded calcrete paleosols

Site formation processes of open-air sites in the humid tropics are often complex due to the high biological activity and marked periodic changes in humidity and temperature in these environments (Friesem et al., 2016; Wright et al., 2017; Morley and Goldberg, 2017). Such complexities can confound clear

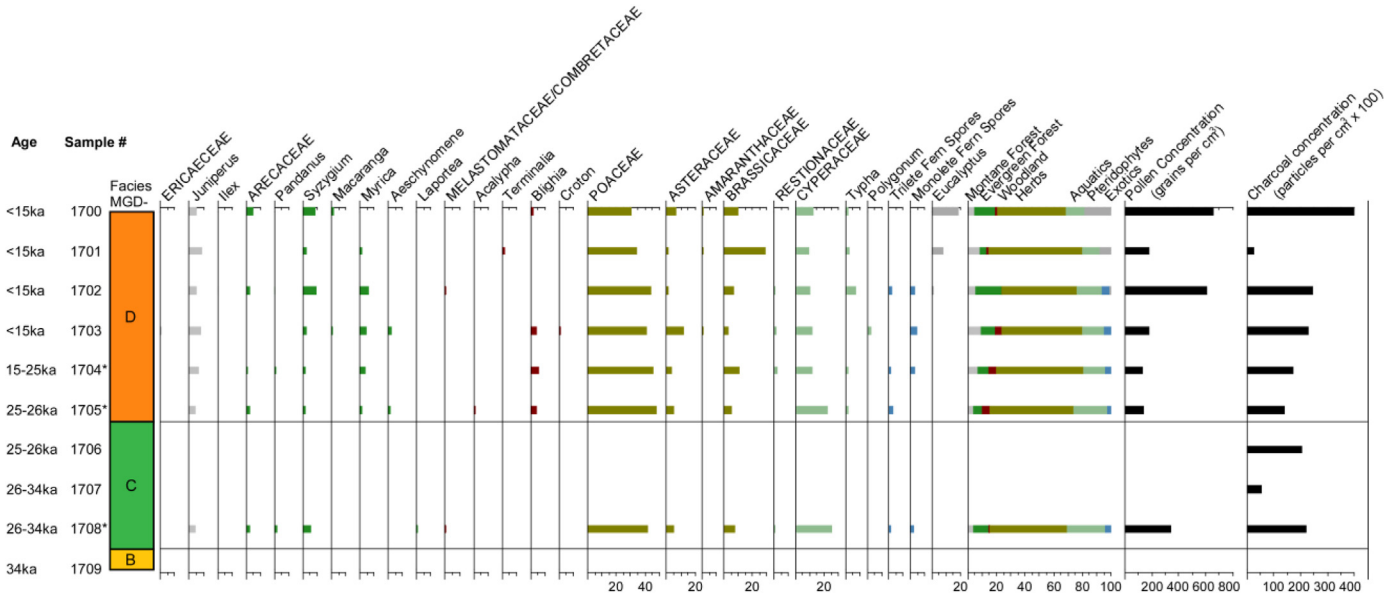

Fig. 8. Pollen diagram with ages and facies indicated on the left and right. Graph created using the Tilia pollen diagram software (Grimm, 2004). Asterisks indicate samples with both pollen and phytolith results available.

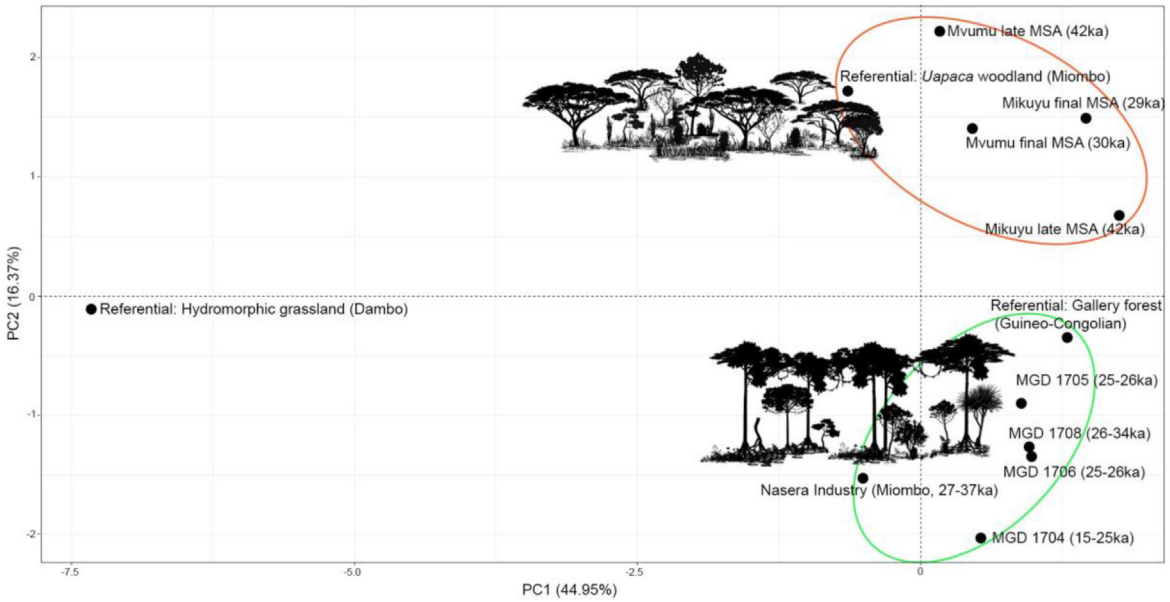

Fig. 9. Principal Component Analysis of MGD-I phytoliths along with penecontemporaneous regional sites. The ellipses group woodland (brown) and forest environments (green). (For interpretation of the references to color in this figure legend, the reader is referred to the Web version of this article.)

interpretations of past human behavior and the environments in which they occurred. The deposits at MGD and BRU have been subject to various post-depositional alterations, including pedogenic and biogenic mixing, the formation of authigenic clay and silt, precipitation of carbonates and iron-manganese, and the formation of redoximorphic features resulting from fluctuations in the groundwater table. Both lateritic soils and carbonate paleosol horizons are the result of prolonged formation histories.

4.2.1. Lateritic soils

Lateritic soils have formed in many parts of the Chitimwe alluvial fan deposits of the Karonga area, especially where the removal of protecting tree cover has encouraged their development (Thompson et al., 2021b). The laterites represent a late phase of soil formation, overprinting earlier pedogenetic phases which typically involved clay illuviation, as seen for example at Chaminade-II (Wright et al., 2017). At BRU, the laterites of facies *BRU-C* exhibit a wider variety of features related to mineral weathering than at the excavations at Chaminade (Wright et al., 2017; Nightingale et al., 2019), possibly due to different sedimentary sources including alkali granite, sandstone, and gneiss. Much of the clay and silt appears to have formed in situ by chemical and physical mineral weathering. Bt horizons in the alluvial fan deposits (facies *BRU-C*) contain various types of clay coatings which are frequently

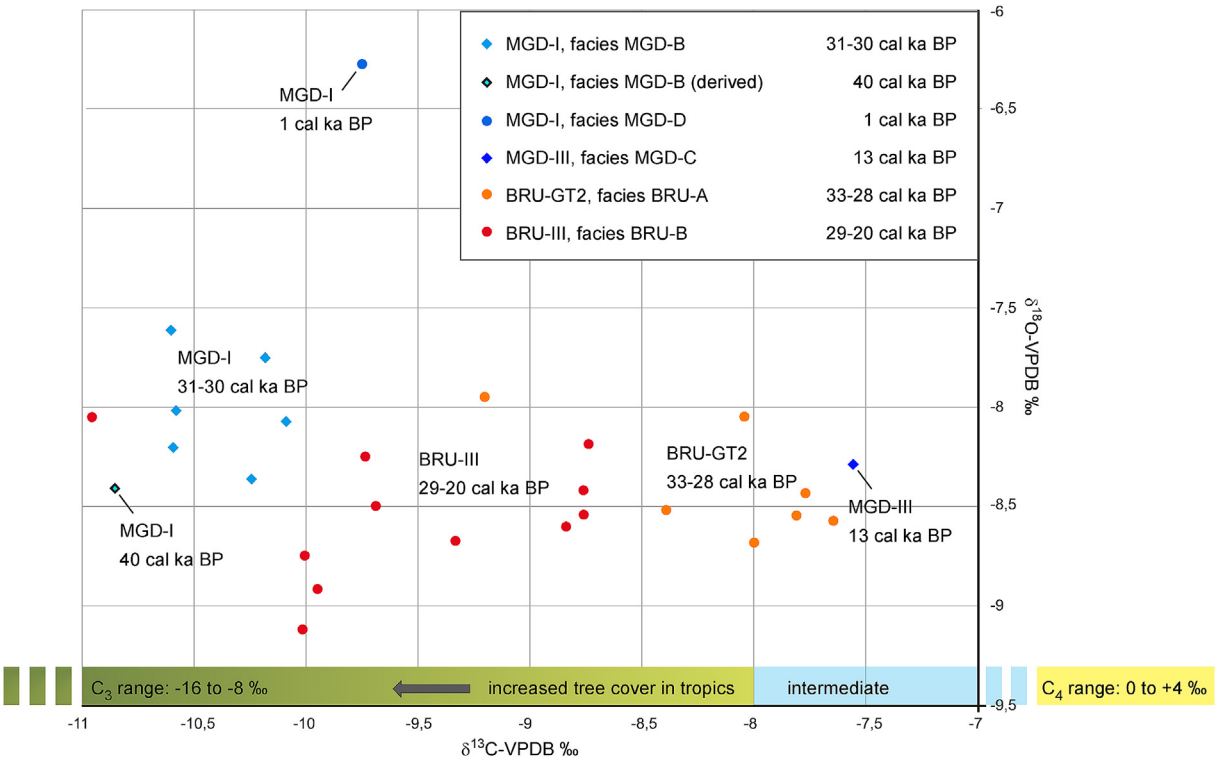

Fig. 10. Scatterplot of the $\delta^{13}C_{PC}$ and $\delta^{18}O_{PC}$ values (both presented relative to VPDB) from carbonate nodules organized according to facies with the ranges of radiocarbon dates indicating the time of their formation, *ante quem*. Radiocarbon ages were calibrated in OxCal v.4.4 (Ramsey et al., 2013) using the SHCal20 atmospheric curve (Hogg et al., 2020). The bar at the bottom on the x-axis shows the ranges of C_3 and C_4 vegetation, with more negative $\delta^{13}C_{PC}$ values associated with denser tree cover. The original isotopic compositions in organic matter, prior to carbonate formation, are between −20‰ and −35‰ for plants following the C_3 photosynthetic pathway, and between −9‰ and −17‰ or plants following the C_4 photosynthetic pathway (Cerling and Quade, 1993). Due to fractionation, pedogenic carbonates forming below C_3 vegetation have values between −16‰ and −8‰, and C_4 vegetation, shown in yellow, has values between 0‰ and +4‰. The values for C_4 vegetation lie to the right from the shown ranges on the x-axis of the scatterplot (−7‰ to −11‰ δ^{13}C-VPDB), and the distance has been truncated for presentation purposes. (For interpretation of the references to color in this figure legend, the reader is referred to the Web version of this article.)

overprinting one another, as well as localized zones with evidence for fracturing and removal of clay coatings by erosional processes within the soil (Fig. 7l-o).

Based on these observations, we hypothesize that *BRU-C* resulted from the cyclic alternation of alluvial deposition, episodes of landform stability during which Bt horizons formed, and erosional events. The Bt horizons may reflect multiple hiatuses in deposition, as indicated by the age range for the aggradation of ten coarse channel beds at BRU-I during Marine Isotope Stage (MIS) 3 that broadly spans from 54 to 29 ka (Fig. 4).

4.2.2. Calcrete paleosols

Carbonate nodules are the most prominent feature of the paleosols at MGD and BRU (*MGD-C, BRU-B*), and also formed in the underlying deposits with less pedogenic development (*MGD-B*, *BRU-A*). Overprinting by carbonate formation has been intensive in these paleosols and deposits, obliterating earlier soil and sedimentary features. Micromorphological and field observations of partly oxidized organic matter and desiccation cracks in facies *MGD-B* and *BRU-A* show that soil formation started when the lake-lagoon began to dry up (Pons and Zonneveld, 1965). This process occurred periodically, probably during the dry season, while the wet season continued to introduce lagoonal sediments which were topped by stream deposits from the alluvial fan. Bioturbation thoroughly mixed the coarse stream deposits with the upper part of the underlying lagoonal clay, creating a welded soil composed of two different types of sediment (Ruhe and Olson, 1980). As the lagoon retreated, more stream deposits buried the paleosol, and clay illuviation (Fig. 7e) and carbonate precipitation (Fig. 6c–f, i) ensued. The overprinting of clay coatings by carbonates demonstrates that these soil processes alternated, probably following seasonal rhythms. Ultimately, carbonate formation became the most dominant process, further enhanced by soil plugging due to the continued growth of carbonate nodules.

Micromorphology and CL-petrography show that carbonate formation occurred in three main ways. (i) The first is especially common in horizons with less pronounced carbonate precipitation (*MGD-D*) and consists of the formation of small (<2 mm) nodules and hypocoatings of micrite. In horizons with more intense carbonate formation, (ii) displacement and disruption of the original sediment fabric (Fig. 6c, 6f-g) and (iii) mineral replacement are more prevalent. The latter is best observed in the calcrete paleosols (*MGD-C*, *BRU-B*) and occurred under extreme alkaline conditions (pH >9), when the opposite trend in solubility of silica and carbonates as a function of pH led to dissolution of siliceous minerals and intense carbonate precipitation (Durand et al., 2010). Within *MGD-C* and *BRU-B*, we observed that carbonates substituted a range of siliceous soil components, including clay domains (e.g., lagoonal clay, Fig. 7c and f), clay coatings, and grains of feldspar and quartz (Alonso et al., 2004; Wright, 2007; Alonso-Zarza and Wright, 2010a; Durand et al., 2010). The process of silicate dissolution and subsequent substitution by calcite is further exemplified by fragmentation (Fig. 7j and k) and brecciation (Fig. 6h) of mineral grains, pseudomorphs or ghost features of replaced minerals within nodules, and residual pore spaces between partly dissolved siliceous grains and the carbonate matrix (Fig. 7g and h) (Alonso et al., 2004).

Depending on the primary material, carbonate replacement resulted in two main types of carbonate nodules:

(i) Nodules formed by replacement of laminated clay, containing fine laminations of silt (Fig. 7b). These nodules of homogeneous micrite are present in all carbonate horizons, but are most typical for the two facies with limited pedogenic development (*MGD-B* and *BRU-A*) (Fig. 7a).
(ii) Nodules formed in the bioturbated portions of the paleosols with abundant coarse sand (*MGD-C* and *BRU-B*), exhibiting zones with different micritic, microsparitic (5-20 μm), and sparitic (>20 μm) crystal sizes and containing various siliceous mineral inclusions such as sand grains, fragments of clay coatings, and clay domains (Fig. 7d). We hypothesize that the frequency and size of these inclusions within the nodules does not only reflect the primary material but may also depend on the maturity of the calcrete, as we expect that increased maturity (continued dissolution and carbonate replacement) will reduce the number and size of the inclusions.

In the literature, nodules comparable to the two types we observed at MGD and BRU are classified into two separate categories: palustrine-pedogenic and calcrete nodules, respectively (Wright, 1990a; Freytet and Verrecchia, 2002). Applying this classification to the nodule types at MGD and BRU, however, could be misleading because the mechanism that formed these pedofeatures is the same, as also supported by carbon and oxygen stable isotope analysis (Fig. 10). Therefore, both nodule types are considered pedogenic carbonates.

The conditions promoting intense carbonate formation at MGD and BRU may have been created by several factors, including the location of the soils within the landscape, the presence of a perched water table, and other climatic conditions such as temperature and precipitation variability. The contribution of carbonate dust was likely not a decisive factor, as carbonate horizons only formed at certain locations within the study area. Namely, the low to middle position in the landscape of the paleosol horizons allowed for soil carbonate in solution, leached from higher parts of the landscape, to be moved into the paleosols and continuously refreshed (Zamanian et al., 2016). In the older, fossiliferous sediments of the Chiwondo Beds, pedogenic carbonates (Lüdecke et al., 2016) and groundwater carbonate (own observations, Fig. S24; Appendix A) are common, but geologic sources for carbonate such as limestone are locally absent, precluding a considerable inherited geogenic input of calcite in the paleosols. This leads us to hypothesize that the supply of calcite and the associated stable isotope values from the nodules indeed reflect the local environment at MGD and BRU. A second formation factor is the poor permeability of the lagoonal clays, which would have caused water to stagnate during heavy (seasonal) rain, forming a perched water table in which water pooled at shallow depths. This groundwater aquitard may have played an essential role in transporting carbonate-saturated waters laterally into the surrounding subsoils, facilitating carbonate precipitation in the capillary zone. Soil plugging by carbonate formation would have retarded water infiltration once the first carbonates had formed. Despite the important role of the aquitard, these carbonate horizons do not classify as groundwater carbonates as they did not form under continuously saturated conditions (Slate et al., 1996; Alonso-Zarza and Wright, 2010b). While temperatures were not very different from modern values (Woltering et al., 2011), pollen data from Lake Masoko indicate stronger seasonality with long, well-pronounced dry seasons between 34 and 23 cal ka BP (Vincens et al., 2007; Gasse et al., 2008). This may have led to enhanced evapotranspiration and carbonate precipitation in the soil after the rainy season, possibly coinciding with increased plant growth.

As outlined above, the long formation history of the paleosol horizons is evidenced by a range of pedofeatures, which in part predate carbonate formation. Radiocarbon dates on the nodules provide an age for the later end stage of soil formation and the associated episode of ground surface stability. They most likely also date a late phase of calcium carbonate formation within the nodules, creating *ante quem* ages for their formation. Although the amount of time required for the formation of calcretes similar to the paleosols of MGD and BRU varies significantly, a minimum of 10 ka has been suggested for calcretes developed in areas where the geogenic contribution of carbonate is low (Wright, 1990b). This timeframe agrees with our OSL and radiocarbon dating, which show that the carbonate nodules of MGD and BRU are up to 10 ka younger than the sediment in which they formed (see for example MGD-III and BRU-III, Figs. 3 and 4).

4.3. Paleoecology

The general lack of pollen in facies *MGD-B* and *MGD-C* (samples 1706, 1707 and 1709, Fig. 8) may reflect environments that are not conducive to preservation, possibly linked to oxidation, which significantly impacts pollen preservation (Moss, 2013). Palynology indicates that the study region was covered with woodland or savanna vegetation, with high values of grass and consistent presence of arboreal taxa (Fig. 8). Throughout *MGD-D* we observed a decrease in woodland and aquatic taxa, which may reflect a transition from moist (early formation of paleosol *MGD-C*) to drier conditions (stream and mass-wasting deposits, *MGD-D*). The top three samples from *MGD-D* (1700–1702, Fig. 8) may reflect the influence of Iron Age or historical agricultural activity, with a clear decline in pteridophytes and increase in Brassicaceae (particularly sample 1701). In addition, the presence of exotic species of the genus *Eucalyptus* in the top of the profile down to ca. 30 cm of depth (1700–1702, Figs. 3 and 8) does not necessarily signal the continuous presence of this vegetational component but rather pollen grains migrating through the soil profile by bioturbation.

The micro-charcoal records suggest frequent fires on the landscape (Fig. 8). The sharp increase in micro-charcoals in the topmost sample (1700) from *MGD-D* potentially reflects changes in fire regimes, associated with the presence of the fire tolerant *Eucalyptus*.

Previous phytolith work has confirmed that for the most part soil phytoliths represent catchment areas smaller than 5 ha (Blinnikov, 1994; Fredlund and Tieszen, 1994; Blinnikov et al., 2002). Therefore, unlike the pollen and micro-charcoals, phytolith data can be used to reconstruct local or semi-local environments. The richest phytolith morphotypes from MGD are similar to dominant phytoliths in the modern regional soil and botanical record (Fig. S5; Appendix A) (Mercader et al. 2019; Mercader et al., 2021a,b), with closest comparison in paleoenvironments of the woodland ecozone. PCA analysis (Fig. 9) shows that between ~34 ka and 15 ka, when late and final MSA groups inhabited MGD, this area or its surroundings consisted of mesic environments similar to the modern evergreen gallery forest, forming along rivers and wetlands, and miombo woodland, widespread in southern central Africa and characterized by the presence of trees of the *Brachystegia* and *Julbernardia* species. This conclusion contrasts somewhat with the reconstruction based on the pollen data, which besides the presence of trees emphasizes a dominance of grasses (Poaceae) and sedges (Cyperaceae). Such discrepancy, however, can be explained by the different scales of the two archaeobotanical methods, with the pollen deriving from a wider, regional catchment.

Stable isotopes from pedogenic carbonate nodules provide even more local, on-site environmental signatures. All $\delta^{13}C_{PC}$ values

consistently fall within the range of the C_3 photosynthetic pathway (Fig. 10), generally associated with closed woodland environments (Cerling, 2009). $\delta^{13}C_{PC}$ values cluster per carbonate soil horizon (Fig. 10), but variation can be noted between different horizons. The carbonate horizons of BRU-GT2 (~33-28 cal ka BP) and MGD-I (~31-30 cal ka BP) overlap in age and formed when MSA hunter-gatherers were present at BRU. Our $\delta^{13}C_{PC}$ data suggest a more open vegetation regime at BRU at this time than at MGD, where tree-cover has generally been denser (Fig. 10). This open woodland at BRU was followed by an increase in tree cover, with the younger carbonate nodules from BRU-III (~29-20 cal ka BP) indicative of more C_3-dominant vegetation, which agrees with the phytolith data from MGD (Figs. 9 and 10).

4.3.1. Broader environmental context

Regional-scale reconstructions of vegetation and paleoenvironments at the end of MIS3 and during MIS2 are available from cores from Lake Malawi (core 1C, central basin) (Debusk, 1998; Beuning et al., 2011; Stone et al., 2011) and the maar-lake of Masoko, located 70 km north from MGD and BRU (Garcin et al., 2006; Vincens et al., 2007). Currently, Lake Malawi is at its highest level within the last 1.3 million years. Diatom records from Lake Malawi suggest deep but fluctuating lake levels between 70 and 55 ka (Stone et al., 2011). Stone et al. (2011) further reconstructed a significant drop in lake level between 47 and 30 ka, in agreement with pollen records indicative of an extremely dry phase between 43 and 40 cal ka BP (Debusk, 1998). Our reconstructions of MGD and BRU indicate that the lake-lagoon formed after ~58 ka, and before ~41 ka. The approach of a lagoon to these sites, which are today located ~6 km inland (Fig. 1), may have been caused by a change in base-level and geometry of the shore deposits, leading to a relative rise in lake level and flooding of the area. After ~41 ka, a shift to drier climate with longer dry seasons may have played a role in the recession of the lake margins and the formation of a seasonal wetland with palustrine-pedogenic carbonates.

Between 34 and 23 cal ka BP, a dry climate characterized by longer dry seasons and open savanna vegetation is indicated by pollen spectra from Lake Masoko. This phase was followed by a period with increasing rainfall and shorter dry seasons with less pronounced seasonality between 23 and 19 cal ka BP (Vincens et al., 2007; Gasse et al., 2008). The marked dry season detected from the early phase of the pollen record of Lake Masoko may have been a key factor in calcrete formation at MGD and BRU, which was most pronounced between 33 and 20 cal ka BP (Fig. 10). Seasonal aridity may also have driven people to MGD and BRU, where streams or places with permanent water, such as the modern springs found near the sites, may have created attractive areas, additionally providing lithic raw materials from pebble and cobble deposits.

4.4. Environments, late MSA occurrences, and forager behaviors

Based on our geoarchaeological and paleoecological analyses, six stages of landscape development leading to the formation of MGD and BRU could be identified. Here we outline these environments in chronological order and contextualize the archaeological occurrences associated with them.

(1) Alluvial fan (~58 ka, *MGD-A*, and by at least ~54 ka at *BRU-C*)

Non-lateritic alluvial fan deposits at MGD (facies *MGD-A*) underlie lagoonal clays (*MGD-B*). Their age (58 ± 9 ka) overlaps with the earliest ages of alluvial fan sedimentation at BRU (Fig. 4), demonstrating that both sites consisted of a terrestrial, alluvial fan landscape before they were flooded by a lake-lagoon. This timing is in line with previous studies, which reconstructed that early Chitimwe alluvial fan deposition was active by 92 ka (Thompson et al., 2021b). Our field observations indicate that no significant landform stability occurred during the formation of the early alluvial fan deposits at MGD (*MGD-A)*, as they exhibit minimal pedogenic development. This further supports interpretations by Thompson et al. (2021b), who argue for an increase in the scale and scope of human occupation and anthropogenic burning after 70 ka, which enhanced alluvial fan activity and contributed to burial of MSA artifacts such as those recovered in the test pits at BRU.

(2) Lagoon (after ~58 ka and before 41 ka, *BRU-A* and *MGD-B*)

MGD and part of BRU became flooded by a non-turbid body of water, such as a lake-lagoon, in which clays intercalated with fine laminations of silt and fine sand. Episodes of alluvial fan aggradation continued at some locations of BRU (BRU-I and BRU-II), signaling a different physical environment from MGD, which was entirely covered by the lagoon. The lagoonal wetlands formed after ~58 ka and well before ~41 ka, based on OSL ages obtained from alluvial fan sediments underlying (*MGD-A*, Fig. 3*)* and overlying (*BRU-C* at BRU-III, Fig. 4) lagoonal clay deposits.

(3) Seasonal wetland (*BRU-A* and *MGD-B*) and late MSA lithic assemblages at BRU (*BRU-C*) (~34-28 ka)

This stage includes episodes of landform stability as well as continued aggradation of alluvial fan deposits (*BRU-C*) at the margins of the lake-lagoon, which was retreating and developing into a seasonal wetland (*BRU-A* and *MGD-B*). Periods of stability are reflected by soil horizons, such as Bt horizons in the alluvial fan deposits (*BRU-C*) and early carbonate nodules forming in the lagoonal deposits (*MGD-B*and *BRU-A*). At MGD, a dense stand of forest cover is indicated by $\delta^{13}C_{PC}$ compositions from carbonate nodules dating to ~40 cal ka BP and ~31-30 cal ka BP, while the isotopic signal from contemporaneous carbonate formation at BRU (BRU-GT2, dating to between ~33 and 28 cal ka BP) indicates a more open vegetation regime, reflecting a patchy, or mosaic landscape (Fig. 10). Pollen assemblages from MGD-I, dating to this time (1708), contain higher amounts of aquatic species and sedges in comparison to the younger samples, but also show presence of evergreens indicative of a forested wetland environment (Fig. 8). The timing of carbonate formation and the corresponding reconstructed vegetation overlap with the age brackets of late MSA occupations on the exposed surfaces of the alluvial fan at BRU (facies *BRU-C*). At BRU-II, two archaeological occurrences were uncovered within the alluvial fan deposits. Few dispersed lithic artifacts were unearthed from sediments dating to between 44 ± 3 ka and 34 ± 3 ka. Additionally, a richer in situ assemblage of sharp-edged late MSA artifacts was found in and on a pebble layer dating to between 34 ± 3 ka and 33 ± 3 ka (Fig. 4), which may represent an ancient, winnowed ground surface. The fact that these occupations bordered facies *BRU-A* and *MGD-B* suggests that foragers at the time used open environments of the alluvial fans adjacent to a seasonal wetland.

(4a) Calcrete paleosol (*BRU-B* and *MGD-C*) (~29-20 cal ka BP, up to ~13 cal ka BP)

Carbonate precipitation ultimately led to the formation of a stage 3 nodular calcrete paleosol (sensu Machette, 1985; Wright, 1990a,b; Durand et al., 2010), dating to between 29 and 20 cal ka BP at BRU (*BRU-B*), with stable carbon isotope compositions indicative of increased tree cover. The calcrete of paleosol *MGD-C* was under-sampled for radiocarbon dating and stable isotope analysis. However, a sample from MGD-III indicates that at this site area carbonate formation continued until ~13 cal ka BP, with stable

carbon isotope compositions reflective of reduced tree cover (Fig. 10). This more open tree cover may indicate an environment created by the processes described in the next stage (4b), which is roughly contemporaneous to 4a.

(4b) Erosion, late "classic" MSA stone tools at MGD, meandering stream (*MGD-D*), and terminal MSA lithic assemblages at MGD (26-15 cal ka BP)

While calcrete formation (stage 4a, facies *MGD-C*) continued in the downhill site areas of MGD, a meandering stream truncated the paleosol at MGD-I, after ~26 ka but before ~15 ka (*MGD-D*, Fig. 3).

Late "classic" MSA lithics were introduced by the meandering stream and deposited with fluvial sands at the base of facies *MGD-D* (Fig. 3). A similar process probably led to the co-occurrence of MSA stone tools and elephant bones in the top 10 cm of the calcrete reported by Clark and Haynes (1970), which likely corresponds to our truncated *MGD-C* paleosol. This hypothesis is supported by the high abrasion of the lithics and elephant bones, which also do not show evidence of forager cutmarks but of crocodile gnawing (Wright et al., 2014).

The fluvial sands with reworked (but unweathered) late "classic" MSA stone tools were buried below a cobble streambed, within the same time bracket of ~26-15 ka. In situ, terminal MSA lithic artifacts with several refits were found embedded in the deposits just above the cobbles and may relate to the approximate level of the ground surface above a Bt horizon detected below the cobbles, which formed during a relatively short period of landform stability (Fig. 6j). With the start of facies *MGD-D,* directly above the truncation, pollen spectra indicate a decline in sedges and aquatic species, and a continuous presence of grasses and evergreens (Fig. 8). Phytolith spectra indicate continuous dense tree cover near MGD, comparable to modern evergreen gallery forest and miombo woodland (Fig. 9).

Overlying the fluvial cobbles and lowermost sands of *MGD-D* are sediments with abundant redeposited soil materials and lagoonal clay deriving from the paleosol of facies *MGD-C*. This reworking of soil materials and fragments of lagoonal clay is indicative of extensive erosion in the area, which may have occurred during mass-wasting events (*MGD-D*) (Fig. 3). Notably, a period of more intensive rainfall is discernible in the lakes Malawi and Masoko between 23 and 11.8 cal ka BP (Vincens et al., 2007; Gasse et al., 2008; Lyons et al., 2015). This more torrential climate may have contributed to erosion, particularly in combination with anthropogenic burning of vegetation cover (Thompson et al., 2021b).

(6) Channels and flash floods, followed by the formation of a winnowed surface (~12−2 ka)

Around 12 ka, a large channel incision truncated the top of the paleosol at MGD-II and MGD-III. More recent infilling (dated to 1865 ± 120 ka at MGD-II and 8200 ± 100 ka at MGD-III) of gravels contains redeposited carbonate nodules, indicating further episodes of high-energy erosion in the area, probably by flash floods. The early Holocene sequences at MGD-II and MGD-III are topped by a winnowed lag deposit which forms the modern ground surface and consists of mixed coarse sediment rich in organic matter from vegetation and human activity.

5. Conclusions

The unique settings of the open-air sites of MGD and BRU at the fringes of the alluvial fan provided the opportunity to reconstruct paleosols and depositional environments absent from sites located on central parts of the fan in the Karonga area. By placing MSA occurrences in their environmental and landscape context, we were able to capture previously unknown aspects of the behavioral spectrum of late MSA foragers.

Though the Karonga area had an increase in occupation after 70 ka (Thompson et al., 2021b), at MGD and BRU we could not gather any evidence of forager occupation until 51 ka. Sediment analysis has shown that, after initial alluvial fan deposition, a lake-lagoon flooded the site areas after 58 ka. This re-configuration of the lake margins has not been reported by previous palaeogeographical and paleoenvironmental reconstructions from Lake Malawi, which were mainly based on drilling and geophysical programs from the lake itself (Scholz et al. 2006, 2011; Cohen et al., 2007; Beuning et al., 2011; Lyons et al., 2015).

MSA hunter-gatherers first visited BRU between 51 and 31 ka when a mosaic of seasonal wetlands was created by the retreating lake-lagoon, which became bordered by alluvial fan deposits. Our paleoenvironmental data show that these MSA people were producing artifacts in forested riparian zones embedded within more open landscapes. The site of MGD attracted MSA human activity only after the formation of a meandering, seasonal stream, which locally opened the landscape after 26 ka. These findings are in line with previous interpretations emerging from our earlier works in the Karonga area, which demonstrated that MSA foragers favored mosaic/riparian landscapes (Thompson et al. 2012, 2018; Wright et al. 2014, 2017; Nightingale et al., 2019).

Data presented in this paper enable us to further expand these reconstructions. The in situ terminal MSA occupation at MGD, dating after 26 ka, is one of the latest intact MSA assemblages known from Africa (Mercader et al., 2012; Barton et al. 2013, 2016; Bader et al., 2018). This indicates that MSA exploitation of gallery forested riparian environments perpetuated into the latest Pleistocene. Our findings reveal that MSA hunter-gatherers might have chosen MGD and BRU not only due to the presence of riparian environments but also because these localities were positioned at the confluence of river and wetland areas, which serve as important corridors for the dispersal of biota (Wantzen et al., 2008). Therefore, MGD and BRU likely offered a wider range of resources to MSA people crucial for their foraging and tool production.

In conclusion, our work demonstrated that a holistic approach integrating geoarchaeological analyses with different ecological proxies can be very effective in achieving multi-scale landscape, environmental, and behavioral reconstructions, even in a dynamic tropical landscape with limited organic preservation. Though extremely complex, future research might target similar depositional environments to benefit from the variety of paleoenvironmental data that can be obtained, as well as the likely presence of MSA hunter-gatherer occupations.

Funding

Funding was provided by the Deutsche Forschungsgemeinschaft (MI 1748/3-1, MI 1748/1-1, and ME 4406/1-1). Fieldwork and analysis were funded by National Geographic-Waitt Foundation grant W115-10, the University of Queensland Archaeological Field School, and the Australian Research Council Discovery Project DP110101305. The Gold Open Access publication of this article was funded by the Interdisciplinary Center for Archaeology and Evolution of Human Behaviour (ICArEHB), through the Foundation for Science and Technology (FCT), project UIDP/04211/2020.

Contributions of co-authors

Christopher Miller: PhD supervisor, DFG grant application, draft review; David Wright: geomorphology/landscape geoarchaeology, OSL, writing; Susan Mentzer: DFG grant application, μ-XRF, draft

review; Julio Mercader: phytolith analysis and interpretation; Patrick Moss: pollen analysis and interpretation; Jeong-Heon Choi: OSL dating; Gunnar Siljedal: phytolith analysis; Siobhán Clarke: phytolith analysis; Aloyce Mwambwiga: phytolith analysis; Kelly Thomas: phytolith analysis; Alvise Barbieri: writing and figures; Potiphar Kaliba: current director of the Malawi Department of Museums and Monuments; Elizabeth Gomani-Chindebvu: previous director of the Malawi Department of Museums and Monuments providing permits at time of excavations; Jessica C. Thompson: PhD co-supervisor, writing, director of MEMSAP excavations and research.

Declaration of competing interest

The authors declare that they have no known competing financial interests or personal relationships that could have appeared to influence the work reported in this paper.

Acknowledgements

We are grateful to Oris Malijani, Joseph Tembo, Frederick Mapemba, Harrison Simfukwe, Chrissy Chiumia, and Malani Chinula at the Malawi Department of Museums and Monuments, as well as Menno Welling of African Heritage Research and Consultancy. We also thank Davie Simengwa, Liton Adhikari, Gervasio Ngumbira, Rachel Warren, Kingsley Pamanda and a local crew including Henry Kalinga, Moses Nyondo, Kondwani Mwafulirwa, Daudi Mwangomba, Gladys Salanga, Violet Chirambo, Frank Kumwenda, Welani Ng'ambi, Petros Mwanganda, Nelson Sichali, Bodwin Kasimba, and many others. Also, thanks to students who joined the University of Queensland Archaeological Field School, and MEMSAP colleagues Sheila Nightingale, Jacob Davis, Andrew Zipkin, Marina Bravo Foster, Scott Robinson, and Victor de Moor. Thanks are owed to Kathy Schick and Nick Toth at the Stone Age Institute for permission to examine the materials from the Cha-1A excavation and for archive photographs, to Andy Cohen at the University of Arizona for access to maps drawn by C.V. Haynes, and to Winston Mwagomba at the Cultural and Museum Centre, Karonga for his excellent memory of passing through the 1966 Cha-1A excavations as a child. We would further like to thank Panagiotis Kritikakis, Peter Kuehn, Heinrich Taubald, Christoph Wissing, Hervé Bocherens, Christoph Berthold, Carla Hadden, Nicholas Conard, Jian Zhao, Nicole Leonard, Michael Toffolo, Arne Meier, Diogo Spinola, Vera Aldeias, and Nuno Bicho. Finally, we would like to acknowledge the helpful feedback we received during the editorial process, which contributed to the improvement of this work. In memory of Georges Stoops.

Appendix A. Supplementary data

Supplementary data to this article can be found online at https://doi.org/10.1016/j.quascirev.2022.107638.

References

Albert, R.M., Bamford, M.K., Cabanes, D., 2009. Palaeoecological significance of palms at Olduvai Gorge, Tanzania, based on phytolith remains. Quat. Int. 193 (1–2), 41–48. https://doi.org/10.1016/J.QUAINT.2007.06.008.

Albert, R.M., Bamford, M.K., Esteban, I., 2015. Reconstruction of ancient palm vegetation landscapes using a phytolith approach. Quat. Int. 369, 51–66. https://doi.org/10.1016/J.QUAINT.2014.06.067.

Alonso-Zarza, A.M., Wright, V.P., 2010a. Chapter 5 Calcretes. Dev. Sedimentol. 61 (C), 225–267. https://doi.org/10.1016/S0070-4571(09)06105-6.

Alonso-Zarza, A.M., Wright, V.P., 2010b. Chapter 2 Palustrine Carbonates. Dev. Sedimentol. 61 (C), 103–131. https://doi.org/10.1016/S0070-4571(09)06102-0.

Alonso, P., Dorronsoro, C., Egido, J.A., 2004. Carbonatation in palaeosols formed on terraces of the Tormes river basin (Salamanca, Spain). Geoderma 118 (3–4), 261–276. https://doi.org/10.1016/S0016-7061(03)00211-8.

Bader, G.D., Tribolo, C., Conard, N.J., 2018. A return to Umbeli Belli: new insights of recent excavations and implications for the final MSA of eastern South Africa. J Archaeol Sci Rep 21, 733–757. https://doi.org/10.1016/j.jasrep.2018.08.043.

Barboni, D., Bremond, L., 2009. Phytoliths of East African grasses: an assessment of their environmental and taxonomic significance based on floristic data. Rev. Palaeobot. Palynol. 158 (1–2), 29–41. https://doi.org/10.1016/J.REVPALBO.2009.07.002.

Barton, R.N.E., Bouzouggar, A., Collcutt, S.N., Carrión Marco, Y., Clark-Balzan, L., Debenham, N.C., Morales, J., 2016. Reconsidering the MSA to LSA transition at Taforalt Cave (Morocco) in the light of new multi-proxy dating evidence. Quat. Int. 413, 36–49. https://doi.org/10.1016/J.QUAINT.2015.11.085.

Barton, R.N.E., Bouzouggar, A., Hogue, J.T., Lee, S., Collcutt, S.N., Ditchfield, P., 2013. Origins of the Iberomaurusian in NW Africa: new AMS radiocarbon dating of the Middle and Later Stone Age deposits at Taforalt Cave, Morocco. J. Hum. Evol. 65 (3), 266–281. https://doi.org/10.1016/J.JHEVOL.2013.06.003.

Basell, L.S., 2008. Middle Stone Age (MSA) site distributions in eastern Africa and their relationship to Quaternary environmental change, refugia and the evolution of Homo sapiens. Quat. Sci. Rev. 27 (27–28), 2484–2498. https://doi.org/10.1016/J.QUASCIREV.2008.09.010.

Betzler, C., Ring, U., 1995. Sedimentology of the Malawi rift: facies and stratigraphy of the Chiwondo beds, northern Malawi. J. Hum. Evol. 28 (1), 23–35. https://doi.org/10.1006/jhev.1995.1004.

Beuning, K.R.M., Zimmerman, K.A., Ivory, S.J., Cohen, A.S., 2011. Vegetation response to glacial-interglacial climate variability near Lake Malawi in the southern African tropics. Palaeogeogr. Palaeoclimatol. Palaeoecol. 303 (1–4), 81–92. https://doi.org/10.1016/j.palaeo.2010.01.025.

Bicho, N., Haws, J., Raja, M., Madime, O., Gonçalves, C., Cascalheira, J., Benedetti, M., Pereira, T., Aldeias, V., 2016. Middle and Late Stone Age of the Niassa region, northern Mozambique. Preliminary results. Quat. Int. 404, 87–99. https://doi.org/10.1016/j.quaint.2015.09.059.

Blair, T.C., McPherson, J.G., 1994. Alluvial fans processes and forms. In: Geomorphology of Desert Environments. https://doi.org/10.1007/978-1-4020-5719-9J4.

Blinnikov, M., 1994. Phytolith analysis and the Holocene dynamics of alpine vegetation. In: Onipchenko, V., Blinnikov, M. (Eds.), Exp Investig Alp Plant Communities Northwest Caucasus, vol. 115. Zuerich, pp. 23–40.

Blinnikov, M., Busacca, A., Whitlock, C., 2002. Reconstruction of the late Pleistocene grassland of the Columbia basin, Washington, USA, based on phytolith records in loess. Palaeogeogr. Palaeoclimatol. Palaeoecol. 177 (1–2), 77–101. https://doi.org/10.1016/S0031-0182(01)00353-4.

Blokhuis, W.A., Kooistra, M.J., Wilding, L.P., 1990. Micromorphology of cracking clayey soils (vertisols). In: Douglas, L.A. (Ed.), Soil Micromorphol a Basic Appl Sci. Elsevier, pp. 123–148.

Bromage, T.G., Schrenk, F., Juwayeyi, Y.M., 1995. Paleobiogeography of the Malawi rift: age and vertebrate paleontology of the Chiwondo beds, northern Malawi. J. Hum. Evol. 28 (1), 37–57. https://doi.org/10.1006/jhev.1995.1005.

Brooks, A.S., Yellen, J.E., Potts, R., Behrensmeyer, A.K., Deino, A.L., Leslie, D.E., 2018. Long-distance stone transport and pigment use in the earliest Middle Stone Age. Science 360 (6384), 90–94. https://doi.org/10.1126/science.aao2646.

Cerling, T.E., 1984. The stable isotopic composition of modern soil carbonate and its relationship to climate. Earth Planet Sci. Lett. 71 (2), 229–240. https://doi.org/10.1016/0012-821X(84)90089-X.

Cerling, T.E., 2009. Stable carbon isotopes in palaeosol carbonates. In: Palaeoweathering, Palaeosurfaces Relat Cont Depos. John Wiley & Sons, Ltd, pp. 43–60. https://doi.org/10.1002/9781444304190.ch2.

Cerling, T.E., Quade, J., 1993. Stable carbon and oxygen isotopes in soil carbonates. In: Swart, P.K., Lomann, K.C., Mckenzie, J., Savin, S. (Eds.), Clim Chang Cont Isot Rec Vol 78. Geophysica. American Geophysical Union, pp. 217–231. https://doi.org/10.1029/gm078p0217.

Clark, J.D., 1966. Initial investigation of the archeology of Karonga District, Malawi. Am. Anthropol. 68 (2), 67–87. https://doi.org/10.1525/aa.1966.68.2.02a00990.

Clark, J.D., Haynes, C.V., Mawby, J.E., Gautier, A., 1970. Preliminary investigations in Malawi. Quaternaria 13, 305–354.

Clark, J.D., Haynes, C.V., 1970. An elephant butchery site at Mwanganda's Village, Karonga, Malawi, and its relevance for Palaeolithic archaeology. World Archaeol. 1 (3), 390–411. https://doi.org/10.1080/00438243.1970.9979455.

Clark, J.D., Haynes, C.V., Mawby, J.E., 1973. Palaeo-anthropological investigations in the Lake Malawi Rift (1965-66): an interim report. In: Hugot, H.J. (Ed.), Pap Proc 6th Pan-African Congr Prehistory Quat Stud. Dakar, pp. 513–530.

Clark, J.D., Stephens, E.A., Coryndon, S.C., 1966. Pleistocene fossiliferous lake beds of the Malawi (Nyasa) Rift: a preliminary report. Am Anthropol New Ser Recent Stud Paleoanthropology 68 (2), 46–87. https://doi.org/10.1525/aa.1966.68.2.02a00960.

Cohen, A.S., Stone, J.R., Beuning, K.R.M., Park, L.E., Reinthal, P.N., Dettman, D., Scholz, C.A., Johnson, T.C., King, J.W., Talbot, M.R., et al., 2007. Ecological consequences of early Late Pleistocene megadroughts in tropical Africa. Proc. Natl. Acad. Sci. USA 104 (42), 16422–16427. https://doi.org/10.1073/pnas.0703873104.

Collura, L.V., Neumann, K., 2017. Wood and bark phytoliths of West African woody plants. Quat. Int. 434, 142–159. https://doi.org/10.1016/J.QUAINT.2015.12.070.

Color X-rite, M., 2009. Munsell Soil-Color Charts with Genuine Munsell Color Chips. Munsell Color, MI, USA.

Debusk, G.H., 1998. A 37, 500-year pollen record from Lake Malawi and implications for the biogeography of afromontane forests. J. Biogeogr. 25 (3), 479–500. https://doi.org/10.1046/j.1365-2699.1998.2530479.x.

Delvigne, J., Stoops, G., 1990. Morphology of mineral weathering and neoformation. I. Weathering of most common silicates. Dev. Soil Sci. 19, 471–481.
Diaz, N., King, G.E., Valla, P.G., Herman, F., Verrecchia, E.P., 2016. Pedogenic carbonate nodules as soil time archives: challenges and investigations related to OSL dating. Quat. Geochronol. 36, 120–133. https://doi.org/10.1016/j.quageo.2016.08.008.
Dixey, F., 1927. The geology of Nyasaland. Q J Geol Soc 83 (3), 432–447.
Dixey, F., 1930. Stone Implements from the Chitimwe Beds, North Nyasa. Annual Report of the Geological Survey Department, Nyasaland.
Durand, N., Monger, C.H., Canti, M.G., Monger, H.C., Canti, M.G., Monger, C.H., Canti, M.G., 2010. In: Stoops, G., Marcelino, V., Mees, F. (Eds.), Calcium Carbonate Features, first ed. Elsevier B.V. https://doi.org/10.1016/B978-0-444-53156-8.00009-X.
Eichhorn, B., Neumann, K., Garnier, A., 2010. Seed phytoliths in West African Commelinaceae and their potential for palaeoecological studies. Palaeogeogr. Palaeoclimatol. Palaeoecol. 298 (3–4), 300–310. https://doi.org/10.1016/J.PALAEO.2010.10.004.
Fahmy, A.G., 2008. Diversity of lobate phytoliths in grass leaves from the Sahel region, west tropical Africa: tribe paniceae. Plant Systemat. Evol. 270 (1), 1–23. https://doi.org/10.1007/S00606-007-0597-Z.
Fredlund, G.G., Tieszen, L.T., 1994. Modern phytolith assemblages from the north American great plains. J. Biogeogr. 21 (3), 321. https://doi.org/10.2307/2845533.
Freytet, P., Verrecchia, E.P., 2002. Lacustrine and palustrine carbonate petrography: an overview. J. Paleolimnol. 27 (2), 221–237. https://doi.org/10.1023/A:1014263722766.
Friesem, D.E., Lavi, N., Madella, M., Ajithprasad, P., French, C., 2016. Site formation processes and hunter-gatherers use of space in a tropical environment: a geo-ethnoarchaeological approach from South India. PLoS One 11 (10), 164185. https://doi.org/10.1371/journal.pone.0164185.
Garcin, Y., Williamson, D., Taieb, M., Vincens, A., Mathé, P.E., Majule, A., 2006. Centennial to millennial changes in maar-lake deposition during the last 45,000 years in tropical Southern Africa (Lake Masoko, Tanzania). Palaeogeogr. Palaeoclimatol. Palaeoecol. 239 (3–4), 334–354. https://doi.org/10.1016/j.palaeo.2006.02.002.
Gasse, F., Chalié, F., Vincens, A., Williams, M.A.J., Williamson, D., 2008. Climatic patterns in equatorial and southern Africa from 30,000 to 10,000 years ago reconstructed from terrestrial and near-shore proxy data. Quat. Sci. Rev. 27 (25–26), 2316–2340. https://doi.org/10.1016/j.quascirev.2008.08.027.
Grimm, E.C., 2004. TGViewVersion2.0.2. Illinois State Museum Research Collection Center, Springfield.
Hogg, A.G., Heaton, T.J., Hua, Q., Palmer, J.G., Turney, C.S., Southon, J., Bayliss, A., Blackwell, P.G., Boswijk, G., Bronk Ramsey, C., et al., 2020. SHCal20 Southern Hemisphere calibration, 0–55,000 years cal BP. Radiocarbon 62 (4), 759–778. https://doi.org/10.1017/RDC.2020.59.
Ivory, S.J., Blome, M.W., King, J.W., McGlue, M.M., Cole, J.E., Cohen, A.S., 2016. Environmental change explains cichlid adaptive radiation at Lake Malawi over the past 1.2 million years. Proc. Natl. Acad. Sci. U. S. A. 113 (42), 11895–11900. https://doi.org/10.1073/pnas.1611028113.
Ivory, S.J., Lezine, A.-M., Vincens, A., Cohen, A., 2018. Waxing and waning of forests: late Quaternary biogeography of southeast Africa. Global Change Biol. 24 (7), 2939–2951. https://doi.org/10.1111/gcb.14150.
Kandel, A.W., Bolus, M., Bretzke, K., Bruch, A.A., Haidle, M.N., Hertler, H., Märker, M., et al., 2016. Increasing Behavioral Flexibility? An Integrative macro-scale Approach to Understanding the Middle Stone Age of Southern Africa. J. Archaeol. Method Theor 23 (2), 623–668. https://doi.org/10.1007/s10816-015-9254-y.
Kaufulu, Z.M., 1990. Sedimentary environments at the Mwanganda site, Malawi. Geoarchaeology - An Int J. 5 (1), 15–27.
Kristensen, J.A., Thomsen, K.J., Murray, A.S., Buylaert, J.P., Jain, M., Breuning-Madsen, H., 2015. Quantification of termite bioturbation in a savannah ecosystem: application of OSL dating. Quat. Geochronol. 30, 334–341. https://doi.org/10.1016/J.QUAGEO.2015.02.026.
Kühn, P., Aguilar, J.A., Miedema, R., 2010. Textural pedofeatures and related horizons. In: Interpret Micromorphol Featur Soils Regoliths. https://doi.org/10.1016/B978-0-444-53156-8.00011-8.
Kullmer, O., 2008. The fossil suidae from the Plio-Pleistocene Chiwondo Beds of northern Malawi, Africa. J. Vertebr. Paleontol. 28 (1), 208–216. https://doi.org/10.1671/0272-4634(2008)28[208:TFSFTP]2.0.CO;2.
Lüdecke, T., Schrenk, F., Thiemeyer, H., Kullmer, O., Bromage, T.G., Sandrock, O., Fiebig, J., Mulch, A., 2016. Persistent C_3 vegetation accompanied Plio-Pleistocene hominin evolution in the Malawi rift (Chiwondo beds, Malawi). J. Hum. Evol. 90, 163–175. https://doi.org/10.1016/j.jhevol.2015.10.014.
Lyons, R.P., Scholz, C.A., Cohen, A.S., King, J.W., Brown, E.T., Ivory, S.J., Johnson, T.C., Deino, A.L., Reinthal, P.N., McGlue, M.M., Blome, M.W., 2015. Continuous 1.3-million-year record of East African hydroclimate, and implications for patterns of evolution and biodiversity. Proc. Natl. Acad. Sci. USA 112 (51), 201512864. https://doi.org/10.1073/pnas.1512864112.
Machette, M.N., 1985. Calcic soils of the southwestern United States. In: Weide, D.L. (Ed.), Soils and Quaternary Geology of the Southwestern United States. Geological Society of America Special Paper 203, pp. 1–22. https://doi.org/10.1130/SPE203-p1.
Mackay, A., Stewart, B.A., Chase, B.M., 2014. Coalescence and fragmentation in the late Pleistocene archaeology of southernmost Africa. J. Hum. Evol. 72, 26–51. https://doi.org/10.1016/j.jhevol.2014.03.003.
Madella, M., Alexandre, A., Ball, T., 2005. International code for phytolith nomenclature 1.0. Ann. Bot. 96 (2), 253–260. https://doi.org/10.1093/AOB/MCI172.
Marcelino, V., Stoops, G., Schaefer, C.E.G.R., 2010. Oxic and related materials. In: Interpret Micromorphol Featur Soils Regoliths, pp. 305–327.
McFarlane, M.J., 1976. Laterite and Landscape. Academic Press, London.
Mentzer, S.M., Quade, J., 2013. Compositional and isotopic analytical methods in archaeological micromorphology. Geoarchaeology 28 (1), 87–97. https://doi.org/10.1002/gea.21425.
Mercader, J., Akuku, P., Boivin, N., Bugumba, R., Bushoz, P., Camacho, A., Carter, T., Clarke, S., Cueva-Temprana, A., Durkin, P., Favreau, J., Fella, K., Haberle, S., Hubbard, S., Inwood, J., Itambu, M., Koromo, S., Lee, P., Mohammed, A., et al., 2021a. Earliest Olduvai hominins exploited unstable environments ~ 2 million years ago. Nat. Commun. 12 (1), 1–15. https://doi.org/10.1038/s41467-020-20176-2.
Mercader, J., Asmerom, Y., Bennett, T., Raja, M., Skinner, A., 2009a. Initial excavation and dating of Ngalue Cave: a Middle Stone Age site along the Niassa Rift, Mozambique. J. Hum. Evol. 57, 63–74. https://doi.org/10.1016/j.jhevol.2009.03.005.
Mercader, J., Astudillo, F., Barkworth, M., Bennett, T., Esselmont, C., Kinyanjui, R., Grossman, D.L., Simpson, S., Walde, D., 2010. Poaceae phytoliths from the Niassa rift, Mozambique. J. Archaeol. Sci. 37 (8), 1953–1967. https://doi.org/10.1016/J.JAS.2010.03.001.
Mercader, J., Bennett, T., Esselmont, C., Simpson, S., Walde, D., 2009b. Phytoliths in woody plants from the miombo woodlands of Mozambique. Ann. Bot. 104 (1), 91–113. https://doi.org/10.1093/AOB/MCP097.
Mercader, J., Bennett, T., Esselmont, C., Simpson, S., Walde, D., 2011. Soil phytoliths from miombo woodlands in Mozambique. Quat. Res. 75 (1), 138–150. https://doi.org/10.1016/J.YQRES.2010.09.008.
Mercader, J., Bennett, T., Esselmont, C., Simpson, S., Walde, D., 2013. Phytoliths from Middle Stone Age habitats in the Mozambican rift (105–29 ka). J. Hum. Evol. 64 (5), 328–336. https://doi.org/10.1016/J.JHEVOL.2012.10.013.
Mercader, J., Clarke, S., Bundala, M., Favreau, J., Inwood, J., Itambu, M., Larter, F., Lee, P., Lewiski-McQuaid, G., Mollel, N., et al., 2019. Soil and plant phytoliths from the Acacia-Commiphora mosaics at Oldupai Gorge (Tanzania). PeerJ 7, e8211. https://doi.org/10.7717/peerj.8211.
Mercader, J., Clarke, S., Itambu, M., Mohamed, A., Mwitondi, M., Siljedal, G., Soto, M., Bushozi, P., 2021b. Phytolith palaeoenvironments at Mumba rock shelter. Front Ecol Evol 9, 699609. https://doi.org/10.3389/FEVO.2021.699609.
Mercader, J., Gosse, J.C., Bennett, T., Hidy, A.J., Rood, D.H., 2012. Cosmogenic nuclide age constraints on Middle Stone Age lithics from Niassa, Mozambique. Quat. Sci. Rev. 47, 116–130. https://doi.org/10.1016/j.quascirev.2012.05.018.
Middleton, G.V., 1973. Johannes Walther's law of the correlation of facies. Geol. Soc. Am. Bull. 84, 979–988.
Morley, M.W., Goldberg, P., 2017. Geoarchaeological research in the humid tropics: a global perspective. J. Archaeol. Sci. 77, 1–9. https://doi.org/10.1016/J.JAS.2016.11.002.
Moss, P.T., 2013. Palynology and its application to geomorphology. Treatise Geomorphol 14, 315–325. https://doi.org/10.1016/B978-0-12-374739-6.00395-X.
Neumann, K., Fahmy, A., Lespez, L., Ballouche, A., Huysecom, E., 2009. The early Holocene palaeoenvironment of Ounjougou (Mali): phytoliths in a multiproxy context. Palaeogeogr. Palaeoclimatol. Palaeoecol. 276 (1–4), 87–106. https://doi.org/10.1016/J.PALAEO.2009.03.001.
Neumann, K., Fahmy, A.G., Müller-Scheeßel, N., Schmidt, M., 2017. Taxonomic, ecological and palaeoecological significance of leaf phytoliths in West African grasses. Quat. Int. 434, 15–32. https://doi.org/10.1016/J.QUAINT.2015.11.039.
Nightingale, S., Schilt, F., Thompson, J.C., Wright, D.K., Forman, S., Mercader, J., Moss, P., Clarke, S., Itambu, M., Gomani-Chindebvu, E., Welling, M., 2019. Late Middle Stone Age behavior and environments at Chaminade I (Karonga, Malawi). J Paleolit Archaeol 2 (3), 258–297. https://doi.org/10.1007/s41982-019-00035-3.
Novello, A., Barboni, D., Berti-Equille, L., Mazur, J.C., Poilecot, P., Vignaud, P., 2012. Phytolith signal of aquatic plants and soils in Chad, Central Africa. Rev. Palaeobot. Palynol. 178, 43–58. https://doi.org/10.1016/J.REVPALBO.2012.03.010.
Patalano, R., Hamilton, R., Finestone, E., Amano, N., Heddell-Stevens, P., Itambu, M., Petraglia, M., Roberts, P., 2021. Microhabitat variability in human evolution. Front. Earth Sci. 9, 1208. https://doi.org/10.3389/feart.2021.787669.
Piperno, M., Tagliacozzo, A., 2001. The elephant butchery area at the middle Pleistocene site of Notarchirico (Venosa , Basilicata, Italy). In: The World of Elephants - Proceedings of the First International Congress. Consiglio Nazionale delle Ricerche, Rome, pp. 230–236.
Pons, L.J., Zonneveld, I.S., 1965. Soil Ripening and Soil Classification: Initial Soil Formation of Alluvial Deposits with a Classification of the Resulting Soils. Veenman, Wageningen.
Ramsey, C.B., Scott, E.M., van der Plicht, J., 2013. Calibration for archaeological and environmental terrestrial samples in the time range 26–50 ka cal BP. Radiocarbon 55 (4), 2021–2027. https://doi.org/10.2458/azu_js_rc.55.16935.
Richter, D., Gruen, R., Johannes-Boyau, R., Steele, T.E., Amani, F., Rue, M., 2017. The age of the hominin fossils from Jebel Irhoud, Morocco, and the origins of the Middle Stone Age. Nature 546 (7657), 293–296.
Ring, U., Betzler, C., 1995. Geology of the Malawi rift: kinematic and tectonosedimentary background to the Chiwondo Beds, northern Malawi. J. Hum. Evol. 28 (1), 7–21. https://doi.org/10.1006/jhev.1995.1003.
Ring, U., Betzler, C., Delvaux, D., 1992. Normal vs. strike-slip faulting during rift development in East Africa: the Malawi rift. Geology 20 (11), 1015–1018. https://doi.org/10.1130/0091-7613(1992)020<1015:NVSSFD>2.3.CO;2.

Ruhe, R.V., Olson, C.G., 1980. Soil welding. Soil Sci. 130 (3), 132–139. https://doi.org/10.1097/00010694-198009000-00004.
Runge, F., 1999. The opal phytolith inventory of soils in central Africa —quantities, shapes, classification, and spectra. Rev. Palaeobot. Palynol. 107 (1–2), 23–53. https://doi.org/10.1016/S0034-6667(99)00018-4.
Scerri, E.M., Thomas, M.G., Manica, A., Gunz, P., Stock, J.T., Stringer, C., 2018. Did our species evolve in subdivided populations across Africa, and why does it matter? Trends Ecol. Evol. 33 (8), 582–584. https://doi.org/10.1016/j.tree.2018.05.005.
Scerri, E.M.L., 2017. The North African Middle Stone Age and its place in recent human evolution. Evol. Anthropol. Issues News Rev. 26 (3), 119–135. https://doi.org/10.1002/evan.21527.
Schoeneberger, P.J., Wysocki, D.A., Benham, E.C., Staff, S.S., 2012. Field Book for Describing and Sampling Soils. Version 3. National Resources Conservation Service, National Soil Survey Center, Lincoln, NE. https://doi.org/10.1111/j.1600-0587.2009.05973.x.
Scholz, C.a., Cohen, A.S., Johnson, T.C., King, J.W., Moran, K., 2006. The 2005 Lake Malawi Scientific Drilling Project. Sci. Drill. 2, 17–19. https://doi.org/10.2204/iodp.sd.2.04.2006.
Scholz, C.A., Cohen, A.S., Johnson, T.C., King, J., Talbot, M.R., Brown, E.T., 2011. Scientific drilling in the great rift valley: the 2005 Lake Malawi Scientific Drilling Project - an overview of the past 145,000 years of climate variability in Southern Hemisphere East Africa. Palaeogeogr. Palaeoclimatol. Palaeoecol. 303 (1–4), 3–19. https://doi.org/10.1016/j.palaeo.2010.10.030.
Scholz, C.A., Johnson, T.C., Cohen, A.S., King, J.W., Peck, J.A., Overpeck, J.T., Talbot, M.R., Brown, E.T., Kalindekafe, L., Amoako, P.Y.O., et al., 2007. East African megadroughts between 135 and 75 thousand years ago and bearing on early-modern human origins. Proc. Natl. Acad. Sci. USA 104 (42), 16416–16421. https://doi.org/10.1073/pnas.0703874104.
Slate, J.L., Smith, G.A., Wang, Y., Cerling, T.E., 1996. Carbonate-paleosol genesis in the Plio-Pleistocene St. David Formation, Southeastern Arizona. J. Sediment. Res. 66 (1), 85–94.
Stephens, E.A., 1963. Geological account of the northwest coast of Lake Malawi between Karonga and Lion Point, Malawi. Am. Anthropol. 68 (2), 50–58. https://doi.org/10.1525/aa.1966.68.2.02a00970.
Stone, J.R., Westover, K.S., Cohen, A.S., 2011. Late Pleistocene paleohydrography and diatom paleoecology of the central basin of Lake Malawi, Africa. Palaeogeogr. Palaeoclimatol. Palaeoecol. 303 (1–4), 51–70. https://doi.org/10.1016/j.palaeo.2010.01.012.
Surovell, T.A., Waguespack, N.M., 2008. How many elephant kills are 14? Clovis mammoth and mastodon kills in context. Quat. Int. 191 (1), 82–97. https://doi.org/10.1016/j.quaint.2007.12.001.
Thien, S.J., 1979. A flow diagram for teaching texture by feel analysis. J. Agron. Educ. 8, 54–55.
Thompson, J.C., Mackay, A., de Moor, V., Gomani-Chindebvu, E., 2014. Catchment survey in the Karonga district: a landscape-scale analysis of provisioning and core reduction strategies during the Middle Stone Age of northern Malawi. Afr. Archaeol. Rev. 31 (3), 447–478. https://doi.org/10.1007/s10437-014-9167-2.
Thompson, J.C., Mackay, A., Nightingale, S., Wright, D., Choi, J.H., Welling, M., Blackmore, H., Gomani-Chindebvu, E., 2018. Ecological risk, demography and technological complexity in the Late Pleistocene of northern Malawi: implications for geographical patterning in the Middle Stone Age. J. Quat. Sci. 33 (3), 261–284. https://doi.org/10.1002/jqs.3002.
Thompson, J.C., Mackay, A., Wright, D.K., Welling, M., Greaves, A., Gomani-Chindebvu, E., Simengwa, D., 2012. Renewed investigations into the Middle Stone Age of northern Malawi. Quat. Int. 270, 129–139. https://doi.org/10.1016/j.quaint.2011.12.014.
Thompson, J.C., Welling, M., Gomani-Chindebvu, E., 2013. Using GIS to integrate old and new archaeological data from Stone Age deposits in Karonga, Malawi. Int J Herit Digit Era 2 (4), 611–630. https://doi.org/10.1260/2047-4970.2.4.611.
Thompson, J.C., Wright, D.K., Ivory, S.J., 2021a. The emergence and intensification of early hunter-gatherer niche construction. Evol. Anthropol. 30, 17–27. https://doi.org/10.1002/evan.21877.
Thompson, J.C., Wright, D.K., Ivory, S.J., Choi, J.-H., Nightingale, S., Mackay, A., Schilt, F., Otarola-Castillo, E., Mercader, J., Forman, S., et al., 2021b. Early human impacts and ecosystem reorganization in southern-central Africa. Sci. Adv. 7 (9776), 1–13. https://doi.org/10.1126/sciadv.abf9776. https://advances.sciencemag.org/content/7/19/eabf9776.
Thompson, J.C., Wright, D.K., Nightingale, S., Kaliba, P.M., 2022. Pleistocene archaeology of northern Malawi. In: Beyin, A., Wright David, K., Wilkins, J., Bouzouggar, A., Olszewski, D. (Eds.), Handb Pleistocene Archaeol Africa Hominin Behav Geogr Chronol. Springer (in press).
Tryon, C.A., 2019. The Middle/Later Stone Age transition and cultural dynamics of late Pleistocene East Africa. Evol. Anthropol. 28 (5), 267–282. https://doi.org/10.1002/evan.21802.
Vincens, A., Garcin, Y., Buchet, G., 2007. Influence of rainfall seasonality on African lowland vegetation during the Late Quaternary: pollen evidence from Lake Masoko, Tanzania. J. Biogeogr. 34 (7), 1274–1288. https://doi.org/10.1111/j.1365-2699.2007.01698.x.
Wadley, L., 2015. Those marvellous millennia: the Middle Stone Age of southern Africa. Archaeol Res Africa 50 (2), 155–226. https://doi.org/10.1080/0067270X.2015.1039236.
Walther, J., 1894. In: Fischer, Bd 3. G. (Ed.), Einleitung in die Geologie als historische Wissenschaft (Jena).
Wantzen, K.M., Yule, C.M., Tockner, K., Junk, W.J., 2008. Riparian wetlands of tropical streams. Trop Stream Ecol 199–217. https://doi.org/10.1016/B978-012088449-0.50009-1.
Woltering, M., Johnson, T.C., Werne, J.P., Schouten, S., Sinninghe Damsté, J.S., 2011. Late Pleistocene temperature history of southeast Africa: a TEX86 temperature record from Lake Malawi. Palaeogeogr. Palaeoclimatol. Palaeoecol. 303 (1–4), 93–102. https://doi.org/10.1016/j.palaeo.2010.02.013.
Wright, D.K., Thompson, J., Mackay, A., Welling, M., Forman, S.L., Price, G., Zhao, J xin, Cohen, A.S., Malijani, O., Gomani-Chindebvu, E., 2014. Renewed geo-archaeological investigations of Mwanganda's village (elephant butchery site), Karonga, Malawi. Geoarchaeology 29 (2), 98–120. https://doi.org/10.1002/gea.21469.
Wright, D.K., Thompson, J.C., Schilt, F., Cohen, A.S., Choi, J.H., Mercader, J., Nightingale, S., Miller, C.E., Mentzer, S.M., Walde, D., et al., 2017. Approaches to Middle Stone Age landscape archaeology in tropical Africa. J. Archaeol. Sci. 77, 64–77. https://doi.org/10.1016/j.jas.2016.01.014.
Wright, V.P., 1990a. A micromorphological classification of fossil and recent calcic and petrocalcic microstructures. Dev. Soil Sci. 19 (C), 401–407. https://doi.org/10.1016/S0166-2481(08)70354-4.
Wright, V.P., 1990b. Estimating rates of calcrete formation and sediment accretion in ancient alluvial deposits. Geol. Mag. 127 (3), 273–276. https://doi.org/10.1017/S0016756800014539.
Wright, V.P., 2007. Calcrete. In: Nash, D.J., McLaren, S.J. (Eds.), Geochemical Sediments and Landscapes. Blackwell Publishing Ltd, pp. 10–45.
Yravedra, J., Rubio-Jara, S., Panera, J., Uribelarrea, D., Pérez-González, A., 2012. Elephants and subsistence. Evidence of the human exploitation of extremely large mammal bones from the Middle Palaeolithic site of Preresa (Madrid, Spain). J. Archaeol. Sci. 39 (4), 1063–1071. https://doi.org/10.1016/j.jas.2011.12.004.
Zamanian, K., Pustovoytov, K., Kuzyakov, Y., 2016. Pedogenic carbonates: forms and formation processes. Earth Sci. Rev. 157, 1–17. https://doi.org/10.1016/j.earscirev.2016.03.003.